

Selection of AGN candidates in the GOODS-South Field through SPITZER/MIPS 24 μm variability

Judit García-González,¹ Almudena Alonso-Herrero,^{1,2} Pablo G. Pérez-González,³ Antonio Hernán-Caballero,¹ Vicki L. Sarajedini,⁴ and Víctor Villar³

¹ *Instituto de Física de Cantabria, CSIC-UC, Avenida de los Castros s/n, 39005 Santander, Spain*

² *Augusto González Linares Senior Research Fellow*

³ *Departamento de Astrofísica, Facultad de CC. Físicas, Universidad Complutense de Madrid, 28040 Madrid, Spain*

⁴ *Department of Astronomy, University of Florida, Gainesville, FL 32611, USA*

ABSTRACT

We present a study of galaxies showing mid-infrared variability in data taken in the deepest *Spitzer/MIPS* 24 μm surveys in the GOODS-South field. We divide the dataset in epochs and subepochs to study the long-term (months-years) and the short-term (days) variability. We use a χ^2 -statistics method to select AGN candidates with a probability $\leq 1\%$ that the observed variability is due to statistical errors alone. We find 39 (1.7% of the parent sample) sources that show long-term variability and 55 (2.2% of the parent sample) showing short-term variability. That is, 0.03 sources $\times \text{arcmin}^{-2}$ for both, long-term and short-term variable sources. After removing the expected number of false positives inherent to the method, the estimated percentages are 1.0% and 1.4% of the parent sample for the long-term and short-term respectively. We compare our candidates with AGN selected in the X-ray and radio bands, and AGN candidates selected by their IR emission. Approximately, 50% of the MIPS 24 μm variable sources would be identified as AGN with these other methods. Therefore, MIPS 24 μm variability is a new method to identify AGN candidates, possibly dust obscured and low luminosity AGN, that might be missed by other methods. However, the contribution of the MIPS 24 μm variable identified AGN to the general AGN population is small ($\leq 13\%$) in GOODS-South.

Key words: galaxies:active-infrared:galaxies

1 INTRODUCTION

Supermassive black holes (SMBH) ($M_{\text{SMBH}} > 10^6 M_{\odot}$) are believed to exist in the center of all galaxies containing a significant bulge component (Kormendy & Richstone 1995). Furthermore, the bulge properties, such as stellar mass and velocity dispersion, are correlated with the black hole mass (Magorrian et al. 1998; Marconi & Hunt 2003; Häring & Rix 2004). From these relations one may deduce that the bulges of the galaxies and the supermassive black holes evolve together, probably mutually regulating each other, or at least, sharing formation and growing mechanisms (see Alexander & Hickox 2012 for a review).

In order to study the connection between galaxy and SMBH formation, we must study those galaxies where the SMBH is growing. This phenomenon is revealed in a variety of ways and it is generally referred to as active galactic nucleus or AGN. There are different methods to identify AGN. Conventionally, the most direct and used one has been optical spectroscopy (Baldwin, Phillips & Terlevich 1981;

Veilleux & Osterbrock 1987). AGN can be identified through the presence of broad lines ($\text{FWHM} \gtrsim 1000 \text{ km s}^{-1}$, Type 1 AGN) or by narrow lines ($\text{FWHM} \lesssim 1000 \text{ km s}^{-1}$) and line ratios in diagnostic diagrams such as $[\text{OIII}]/\text{H}\beta$ vs $[\text{NII}]/\text{H}\alpha$ (Type 2 AGN). Unfortunately, spectroscopy of a large number of objects is very expensive in terms of observing time, especially for faint sources in cosmological fields. Furthermore, AGN lines can be obscured and/or swamped by emission from the host galaxy (Moran, Filippenko & Chornock 2002).

AGN in cosmological fields are routinely identified by their X-ray emission (Alexander et al. 2003; Brandt & Hasinger 2005), mid-infrared (IR) emission (Lacy et al. 2004; Stern et al. 2005; Alonso-Herrero et al. 2006; Donley et al. 2012; Mateos et al. 2012; Stern et al. 2012; Assef et al. 2013; Lacy et al. 2013), excess radio emission (Donley et al. 2005; Del Moro et al. 2013), and combinations of different emissions (e.g., Martínez-Sansigre et al. 2005). All these methods present their own biases. For example, only about 10% of the

optically selected QSO are detected as radio sources (Smith & Wright 1980), and in general there is little overlap between radio and IR/X-ray selected AGN (Hickox et al. 2009). X-ray surveys may miss the most obscured AGN needed to fit the cosmic X-ray background (Gilli et al. 2007). The IR methods, on the other hand, are only complete for the most luminous AGN (e.g., Donley et al. 2012), but they are likely to select obscured AGN not detected in X-rays (Mateos et al. 2013).

Variability can also be used to select AGN. Practically all AGN vary on time-scales from hours to millions of years (Ulrich, Maraschi & Urry 1997; Hickox et al. 2014). Any variability detected in galaxies on human time-scales must originate in the nuclear region, because the typical timescale for star formation variability is ≥ 100 Myr (Hickox et al. 2014). In particular low-luminosity AGN are expected to show stronger variability than the luminous ones (Trevese et al. 1994). Therefore, variability is likely to be an effective method to select low-luminosity AGN. Although the mechanisms that produce variability are not well understood, the main explanations involve disk instabilities (Pereyra et al. 2006) or changes in the amount of accreting material (Hopkins & Beacom 2006).

All these methods of AGN selection are complementary and each one can detect sources other methods miss. It is therefore important to study the same region of the sky with different methods of AGN selection.

In the last decade a number of studies have identified AGN in the Great Observatory Origins Deep Survey (GOODS; Giavalisco et al. 2004) fields. The GOODS fields are two fields of 150 arcmin^2 centered around of the Hubble Deep Field North (HDFN; Williams et al. 1996) and the Chandra Deep Field South (CDFS; Giacconi et al. 2001). The observations in the GOODS fields are amongst the deepest at all wavelengths, from X-rays to radio. In particular, these fields have observations from *Spitzer*, *Hubble Space Telescope (HST)*, *Chandra*, *Herschel*, *XMM-Newton* and many ground-based facilities.

There are a number of variability studies in the GOODS fields, most of them using optical data. The first one was made by Sarajedini, Gilliland & Kasm (2003) using *V*-band data ($\lambda_c = 550 \text{ nm}$) from *HST* in two epochs separated by five years. They found nuclear variability evidence in 16 of 217 galaxies (7% of the sample) with magnitudes down to 27.5. Cohen et al. (2006) conducted a similar study using the *HST* *i*-band ($\lambda_c = 775 \text{ nm}$) data from the Hubble Ultra Deep Field (HUDF; Beckwith et al. 2006). They determined that 1% of the sources (45 sources) presented significant variability. Klesman & Sarajedini (2007) conducted a study of five epoch *V*-band data in the GOODS South field. They selected a sample of 22 mid-IR power-law sources (using the criteria of Alonso-Herrero et al. 2006) and 102 X-ray sources and found that 26% of the sample were variable in the optical. Trevese et al. (2008) used ground-based data, also in the *V*-band and obtained 132 variable AGN candidates (2.6% of the sample). Villforth, Koekemoer & Grogan (2010) selected all the objects in the *z*-band ($\lambda_c = 850 \text{ nm}$) catalog in the GOODS fields in five epochs. They found 139 variable AGN candidates ($\sim 1.3\%$ of the sample) in the North and South fields. Sarajedini et al. (2011) identified 85 variable galaxies ($\sim 2\%$ of the sample) in the North and South fields using

five epochs *V*-band images from the *Hubble Space Telescope* Advanced Camera for Surveys.

X-ray variability of low luminosity X-ray sources has also been used to identify additional AGN in the CDFS. Paolillo et al. (2004) studied 346 sources and found that 45% of the sources with more than 100 counts presented X-ray variability. Young et al. (2012) found that 185 of 369 AGN and 20 of 92 galaxies (i.e., low-luminosity AGN with $L_{0.5-8\text{keV}} < 10^{42} \text{ erg s}^{-1}$) presented X-ray variability.

Mooley et al. (2013) studied radio variability in the Extended-CDFS. They found that 1.2% of the point sources presented radio variability associated with the central regions of AGN or star-forming galaxies.

The aim of this paper is to identify AGN through mid-IR variability in the GOODS-South field using $24 \mu\text{m}$ observations taken with the Multiband Imaging Photometer for *Spitzer* (MIPS, Rieke et al. 2004) on board the *Spitzer* Space Telescope (Werner et al. 2004). The near and mid-IR nuclear emission of AGN, once the stellar component is subtracted, is believed to be due to hot and warm dust (200–2000 K) in the dusty torus of the AGN, according to the Unified Model (Antonucci 1993). In this context, variability in the accretion disk emission would cause delayed variability in the near and mid-IR as the hot and warm dust, respectively, in the torus react to this change (see Hönig & Kishimoto 2011 and references therein).

Our choice of using mid-IR variability allows a novel way to select low luminosity and possibly obscured AGN that might be otherwise missed by other techniques. Apart from this work, there is only other IR variability study in the Boötes cosmological field using IRAC data (Kozłowski et al. 2010). They used the most sensitive IRAC bands at 3.6 and $4.5 \mu\text{m}$ and found that 1.1% of the sources satisfied their variability criteria.

The paper is organized as follows: in Section 2 we present the MIR data used to detect variable sources. In Section 3 we explain the procedures followed to get photometry of the data. In Section 4 we present the statistical method used to select the variable candidates. In Section 5 we present the general properties of these candidates, as well as their IRAC properties. In Section 6 we present the candidates in the Extended Chandra Deep Field South (E-CDFS), their properties, and a cross-correlation with other AGN catalogs in the same field. The discussion and conclusions are given in Section 7. Throughout this work we use a cosmology with $H_0 = 70 \text{ km s}^{-1} \text{ Mpc}^{-1}$, $\Omega_m = 0.3$ and $\Omega_\Lambda = 0.7$.

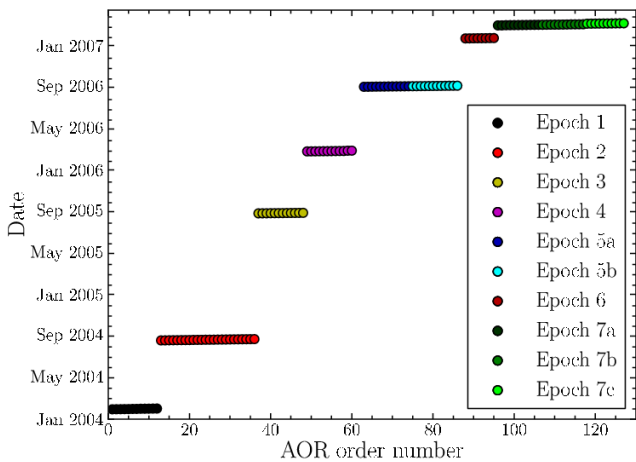
2 THE DATA

We compiled all the data taken around the GOODS South field with the MIPS instrument at $24 \mu\text{m}$ by querying the *Spitzer* Heritage Archive¹. This field was observed by *Spitzer* during several campaigns from January 2004 to March 2007. We focused our study on a region around $\text{RA}=3^{\text{h}}32^{\text{m}}36^{\text{s}}$ (J2000) and $\text{DEC}=-27^\circ48'39''$ (J2000). These data correspond to different observing proposals from different PI, including the Guaranteed Time Observations program (GTO,

¹ <http://sha.ipac.caltech.edu/applications/Spitzer/SHA>

Table 1. MIPS 24 μm observing programs in GOODS-South.

Epoch	PI	Program ID	Program name	Initial date	Final date	AORs ¹	BCDs ²	t_{exp} ³ (s)	Area (arcmin ²)
1	Rieke, G.	81	The Deep Infrared Sky	29-01-2004	01-02-2004	12	7660	10	2653
2	Dickinson, M.	194	Great Observatories Origins Deep Survey (GOODS), continued	19-08-2004	23-08-2004	24	14974	30	255
3	Rieke, G.	81	The Deep Infrared Sky	26-08-2005	28-08-2005	12	6660	10	1706
4	Frayser, D. T.	20147	Ultra-Deep MIPS-70 Imaging of GOODS CDF-S	24-02-2006	26-02-2006	12	19968	10	226
5	Dickinson, M.	30948	A deep-Wide Far-Infrared Survey of Cosmological Star Formation and AGN Activity	01-09-2006	05-09-2006	24	39633	10	756
6	Dickinson, M.	30948	A deep-Wide Far-Infrared Survey of Cosmological Star Formation and AGN Activity	22-01-2007	23-01-2007	8	6216	10	2293
7	Dickinson, M.	30948	A deep-Wide Far-Infrared Survey of Cosmological Star Formation and AGN Activity	01-03-2007	07-03-2007	32	44274	10	2265

¹ AOR: Astronomical Observation Request.² BCD: Basic Calibrated Data.³ t_{exp} : Exposure time per BCD.**Figure 1.** Summary of the different epochs available in the GOODS-South field with deep *Spitzer*/MIPS 24 μm observations. The epochs with the longest durations can also be divided in subepochs to study short-term variability (time scales of days). The number of AORs per epoch and the exposure time per BCD are given in Table 1.

PI: G. Rieke) and the GOODS program (PI: M. Dickinson). We refer the reader to Table 1 for a detailed description of all the MIPS 24 μm observing programs in GOODS-South. We have obtained 151 AORs (Astronomical Observation Request) but only downloaded 127 because the others were from the SWIRE (Spitzer Wide-area InfraRed Extragalactic) survey and were not sufficiently deep. For each epoch and subepoch, we built a mosaic with the AORs using the software MOPEX² provided by the *Spitzer* Science Center (SSC).

² <http://ssc.spitzer.caltech.edu>

We divided these data sets into 7 different epochs in order to detect variable sources (see Figure 1). Epochs 5 and 7, which have the longest durations, can also be divided into subepochs to detect short term variability in time scales of days and even of hours. In Table 1 we list the main information about the epochs. Each epoch has both a different field of view (FoV) and a different depth. As can be seen from Table 1, Epoch 2 has the longest exposure time per Basic Calibrated Data (BCD), resulting in the deepest MIPS 24 μm exposure in our data sets (see below).

For this study we decided to exclude Epochs 2, 4, and 5 because their FoV is small when compared to the other epochs (see Table 1). Figure 2 shows the FoV of Epochs 1, 3, 6, and 7 and how they overlap. The common area for the four epochs is ~ 1360 arcmin². They probe time scales of months up to three years, and henceforth are used to study the long-term variability covering a period of over three years. We also subdivided Epoch 7 in three epochs, namely Epochs 7a, 7b, and 7c to study the short-term variability. The short-term variability epochs have a common area of ~ 1960 arcmin² and probe time scales of days, covering a period of 7 days.

3 MIPS 24 μm PHOTOMETRY

To study the temporal variability of MIPS 24 μm sources detected in the common regions we built a source catalog for each epoch and subepoch. We used SExtractor (Source-Extractor, Bertin & Arnouts 1996) to detect sources and the Image Reduction and Analysis Facility (IRAF)³ to perform the photometry following the procedure explained in

³ IRAF is distributed by the National Optical Astronomy Observatory, which is operated by the Association of Universities for Research in Astronomy (AURA), Inc., under cooperative agreement with the National Science Foundation.

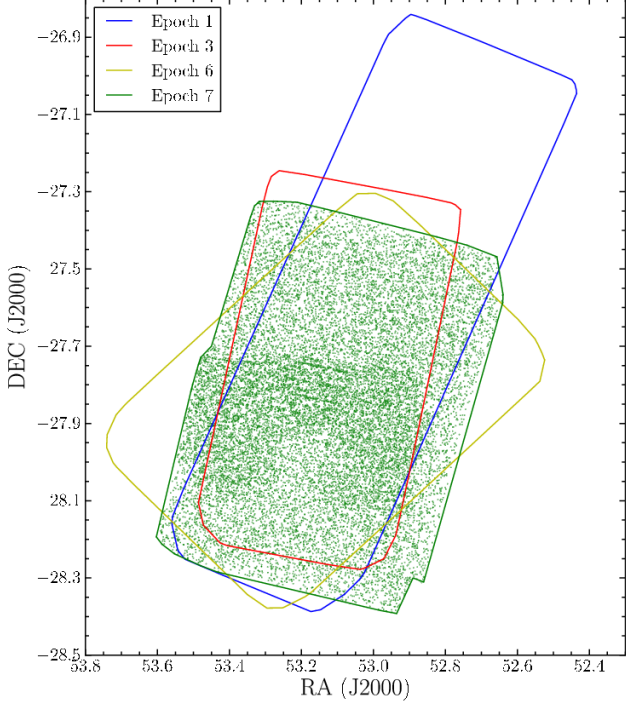


Figure 2. FoV of Epochs 1, 3, 6, and 7, and their overlap region. These four epochs are used to study the long-term variability. Epoch 7 is subdivided in three epochs to study the short-term variability. The filled dots indicate the MIPS 24 μ m sources detected in epoch 7. This epoch is deeper in the center region.

Pérez González et al. (2005, 2008). Sources were detected in five passes to recover the faintest ones, possibly hidden (i.e., more difficult to detect) by brighter sources. All the measurements were made by PSF fitting. To obtain the photometry, we used a circular aperture of radius $\sim 12''$ and then applied an aperture correction of 17% as in Pérez-González et al. (2005) to obtain the total flux. We calculated the uncertainties in the flux taking into account the correlation of the pixel-to-pixel noise introduced by the reduction method and mosaic construction, as described in appendix A.3 of Pérez-González et al. (2008). We obtained a 24 μ m source catalog for each epoch. In this work we restrict the analysis to sources above the 5σ detection limit in the shallowest data in the mosaics. This corresponds to MIPS 24 μ m fluxes of 80 μ Jy and 100 μ Jy for the long-term and the short-term epochs, respectively. We also discarded sources with neighbours at distances of less than $10''$ to minimize crowding effects in the photometry that could affect the flux measurements and produce false variability positives. In Table 2 we list for each epoch the total number of detections, the number of $> 5\sigma$ detections, the number of $> 5\sigma$ detections without neighbours, the area covered, and the density of objects. The positional accuracy of our catalogs is better than $0.7''$.

To identify the common sources in all the epochs we cross-matched the catalogs using a $2''$ radius, imposing additionally that the $2''$ criterion was fulfilled in each pair of

epochs. Due to this criterion, we missed 316 sources cross-matching Epochs 1, 3, 6, and 7 and 282 sources cross-matching Epochs 7a, 7b, and 7c. For the long-term variability (Epochs 1, 3, 6, and 7) there are 2277 sources ($1.67 \text{ objects} \times \text{arcmin}^{-2}$) in common with 24 μ m flux $> 80 \mu\text{Jy}$ (5σ detection) without neighbours within $10''$ and satisfying the $2''$ criterion. For the short-term variability (Epochs 7a, 7b, and 7c) there are 2452 sources ($1.25 \text{ objects} \times \text{arcmin}^{-2}$) in common with 24 μ m flux $> 100 \mu\text{Jy}$ (5σ detection) without neighbours within $10''$ and satisfying the $2''$ criterion. Our final catalogs contain 2277 MIPS 24 μ m sources detected in Epochs 1, 3, 6, and 7 and 2452 MIPS 24 μ m sources in Epochs 7a, 7b, and 7c, covering an area of 1360 and 1960 arcmin^2 , respectively.

4 SELECTION OF MIPS 24 μ m VARIABLE SOURCES

In this section we describe the method used to select the 24 μ m variable sources. To do so we used a χ^2 -statistics method to account for the variations of intrinsic flux uncertainties of each epoch (related to differences in depth). This is the case for our study as different epochs have different depths and within a given mosaic there are some variations in depth. The latter effect is most prominent in epoch 7, which is deeper in the center.

This method associates each flux with its error. The χ^2 -statistics is defined as follows:

$$\chi^2 = \sum_{i=1}^n \frac{(F_i - \bar{F})^2}{\sigma_i^2} \quad (1)$$

where n is the number of epochs, F_i is the flux in a given epoch, σ_i is the associated error in the i^{th} epoch, and \bar{F} is the mean flux.

As errors are essential in this method, we checked them for each epoch. Errors in the parent photometric catalog could be affected by correlation of the noise due to the reduction method. We compared our estimated errors with the uncertainties resulting from the scatter of points with the fluxes estimated in images from different epochs (see Figure A1 and Appendix A). As fluxes in different epochs are measured independently, the scatter must account for the real uncertainties of the measured fluxes. The scatter in this plot is entirely consistent with the photometric errors estimated in Section 3. We refer the reader to Appendix A for more details.

We calculated the χ^2 value for each source without neighbours. We selected as variable candidates those sources above the 99th percentile of the χ^2 distribution expected from photometric errors alone. That is, only 1% of non-variable sources satisfy the selection criteria. This value corresponds to $\chi^2 \geq 11.34$ for the 4 epochs sample (3 degrees of freedom) and $\chi^2 \geq 9.21$ for the 3 epochs one (2 degrees of freedom). In Figure 3 we show the observed χ^2 distribution (filled histograms), the theoretical distribution (black line), and the threshold (red dashed line) for the four epochs (top panel) and three epochs (bottom panel). As can be seen from these figures, the calculated values of χ^2 follow well the expected theoretical distribution for gaussian photometric errors, indicating that our estimates of the flux uncertainties are accurate (see Appendix B for more details).

Table 2. MIPS 24 μm source counts for the different epochs.

Epoch	$N_{\text{detections}}$	$N_{\text{detections}}$ $F > 5\sigma$	$N_{\text{detections}}$ $F > 5\sigma$ without neighbours	Area (arcmin ²)	Density (objects/arcmin ²)
Long-term variability ($5\sigma=80 \mu\text{Jy}$)					
1	19742	11467	8017	2653	3.02
3	11843	7116	5041	1706	2.95
6	15707	9697	6870	2293	3.00
7	18406	9320	6605	2265	2.92
Short-term variability ($5\sigma=100 \mu\text{Jy}$)					
7a	14453	7607	5715	2027	2.82
7b	15629	7348	5551	2107	2.63
7c	14659	7673	5789	2046	2.83

Every object with a χ^2 value higher than the threshold was visually inspected to remove artefacts. We also discarded objects that fell close to the edge of the mosaic. We also compared the candidates with the supernova (SN) catalog of Strolger et al. (2004) and found that none of our candidates was in the SN catalog. The original number of selected variable sources before the removal of artefacts/objects close to the edge of mosaics was 52 and 64 for long-term and short-term variable sources. In the insets of Figure 3 the red histogram shows the distribution for the final candidates. After discarding problematic objects, our final sample contains 39 MIPS 24 μm long-term variable sources ($0.03 \text{ sources} \times \text{arcmin}^{-2}$) and 55 MIPS 24 μm short-term variable sources ($0.03 \text{ sources} \times \text{arcmin}^{-2}$). Only two sources are identified as having both, long and short-term variability. The spatial distribution of the MIPS 24 μm variable sources in the GOODS-South field is shown in Figure 4.

The χ^2 cut means that we would expect that 1% of the parent samples of MIPS 24 μm sources would be incorrectly identified as variable (i.e., false positives). The expected numbers of false positives are then 23 and 25 sources for long and short-term variable sources. Taking the original number of selected variable sources before the removal into account we expect that the fraction of false positives in our final sample of variable sources would be $\sim 44\%$ for long-term and $\sim 39\%$ for short-term. We detect many more variable source candidates than expected by random errors, so our selection is statistically meaningful.

The selected MIPS 24 μm long-term and short-term variable sources represent 1.7 and 2.2% of the original parent samples, respectively. After removing the expected number of false positives, the estimated percentages are 1.0% and 1.4%. These fractions of variable sources at 24 μm are similar to those found in the same cosmological field at other wavelengths, mostly optical and near IR (e.g. Cohen et al. 2006; Villforth et al. 2010; Sarajedini et al. 2011; Kozłowski et al. 2010). The higher fraction of short-term variable sources is due to the presence of a deeper region in Subepochs 7a, 7b, and 7c (shown as the area enclosed by the solid line in Figure 4). This means that the photometric errors of sources in this region are smaller and then if variable, they present higher values of χ^2 than sources in shallower areas.

We note that the presence of intense (obscured) star-formation in the host galaxy would impair the detection of AGN variability at 24 μm , so only sources with the highest

variability might be detected. We refer the reader to Sections 6.1 and 6.3 for further discussion on this issue.

In Appendix C we show an example of the MIPS 24 μm images of four variable sources, two long-term and two short-term, in each of the epochs of our study. In Tables D1 and E1 in the Appendices we list the flux and corresponding error at each epoch, median flux, and χ^2 value, for the long-term and short-term MIPS 24 μm variable sources, respectively.

5 PROPERTIES OF THE MIPS 24 μm VARIABLE SOURCES

In this section we analyze the different properties of the 24 μm variable sources, such as their median 24 μm fluxes, variability properties, and their IRAC colours.

5.1 MIPS 24 μm properties

In Figure 5 we show the distribution of the mean flux (over the 3 or 4 different epochs) at 24 μm for the long-term variable sources (top panel) and short-term variable sources (bottom panel) compared with the corresponding flux distribution of the parent sample for $> 5\sigma$ detections. In both cases, the 24 μm fluxes of the variable sources are dominated by sources with mean fluxes below 300 μJy . The median 24 μm flux is 168 μJy for the long-term variable sources and 209 μJy for the short-term variable sources (see Table 3). This slight difference in the median values of the 24 μm fluxes for long and short-term variability is likely reflecting the different depths (i.e., 5σ detection limits) of the epochs rather than different intrinsic properties of the sources (see Section 6).

We cross-correlated our parent MIPS 24 μm catalogs with the Xue et al. (2011) deep X-ray catalog of AGN and galaxies using a search radius of $2.5''$ (see Section 6.2). There are 211 X-ray sources that are not stars in Xue et al. (2011) catalog detected in 24 μm satisfying our criteria, that is, they have 24 μm fluxes over our 5σ limit and have no neighbours within $10''$. Of the 211 sources, 149 are classified as AGN in the Xue et al. (2011) catalog. These X-ray selected AGN in our parent catalogs have a 24 μm median flux of $\sim 240 \mu\text{Jy}$. This implies that our selected 24 μm variable sources are typically fainter at 24 μm than X-ray selected AGN. Since the redshift distributions are similar (see Section 6.1),

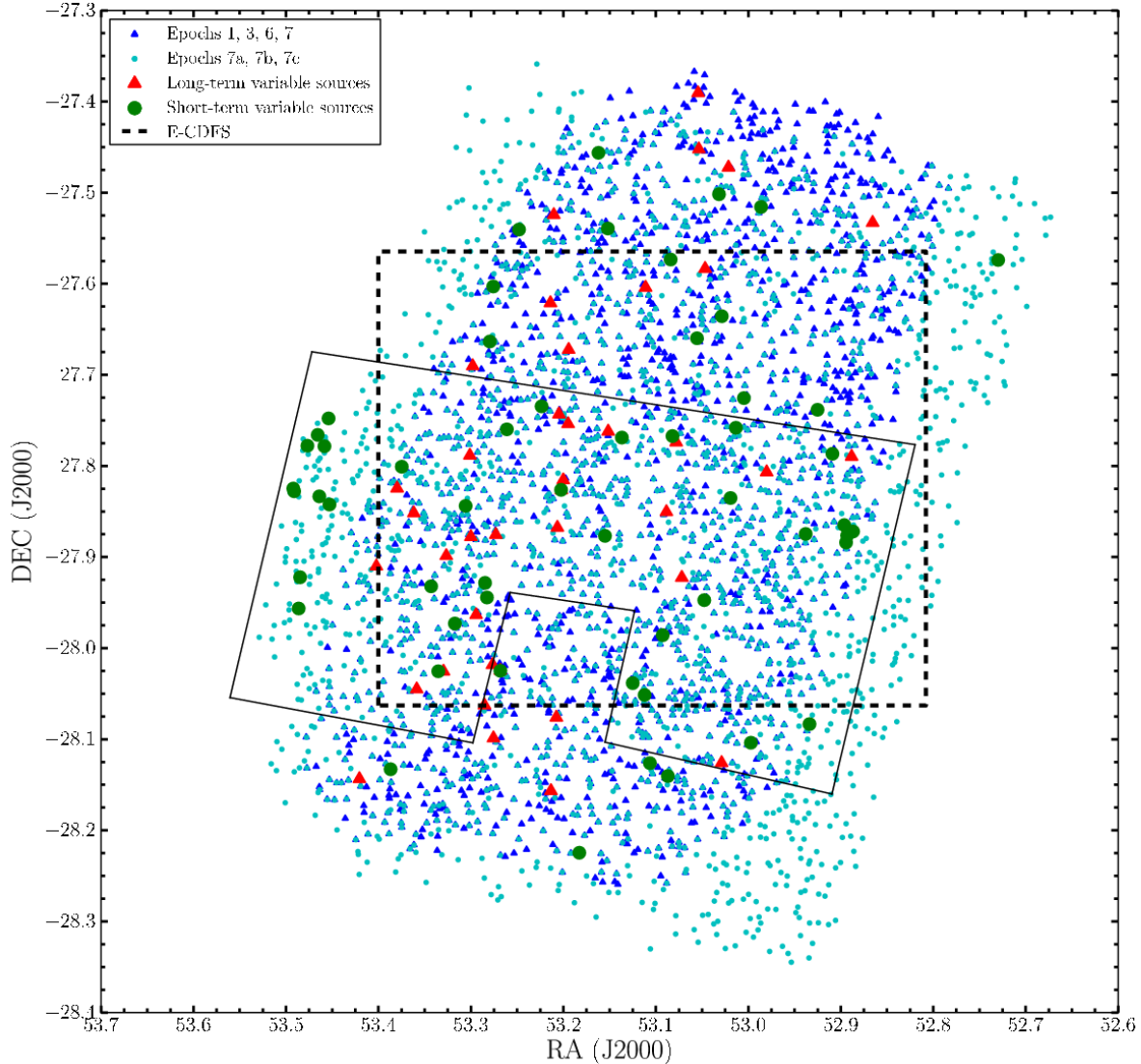


Figure 4. Location of the MIPS 24 μm long-term variable sources (red large triangles) and the short-term variable sources (green large circles) in GOODS-South. The black dashed line encloses the E-CDFS (see Section 5 for more details). The small blue triangles and the small cyan circles are all the MIPS 24 μm common sources to Epochs 1, 3, 6, and 7 and to Epochs 7a, 7b, and 7c, respectively. The solid line encloses the deepest region in Epochs 7a, 7b, and 7c.

this may indicate that the 24 μm variable sources, if they were AGN, are less luminous, as predicted by Trevese et al. (1994).

5.2 Variability Properties

In Figure 6 we show two example light curves, one of long-term and the other of short-term variable sources. Each plot shows the name of the source, the χ^2 value and the measure of the variability Var (see below, Equation 2). The light

curves for all the long and short-term 24 μm variable sources are presented in Appendices F and G, respectively.

As a first measure of the variability, we calculated the maximum to minimum flux ratio, R_{max} , as: $R_{max} = f_{max}/f_{min}$. The long-term and short-term variable sources show similar values of the average and median R_{max} of approximately 1.5 – 1.6 (see Table 3 and Figure 7).

Another estimate of the variability is the ratio between the maximum and minimum values and the mean flux \bar{f} measured as a %.

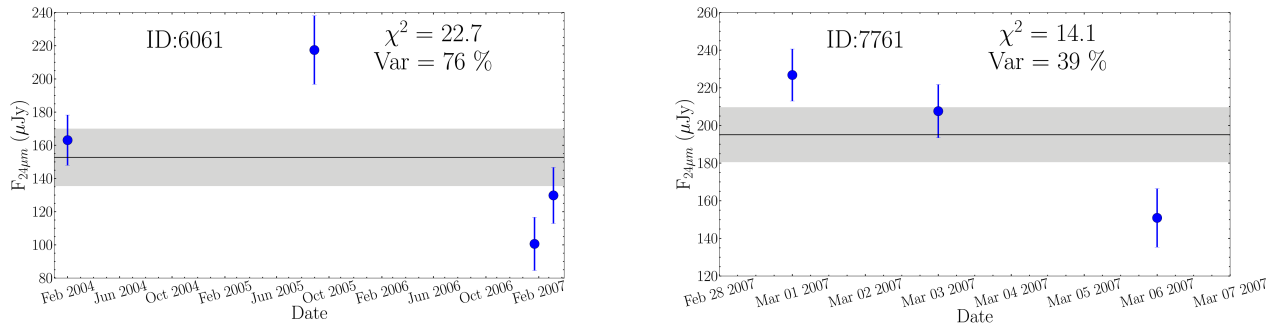


Figure 6. Examples of light curves of two MIPS 24 μm variable sources in GOODS-South. The left panel corresponds to a long-term variable source (four epochs) and the right panel to a short-term variable candidate (three epochs). The flux for each epoch is plotted with its corresponding photometric error. The solid line is the 24 μm mean flux of the source and the gray shaded area is the average of the errors of the source. Each plot lists the name of the source, the χ^2 value, and Var. Light curves for the entire sample of MIPS 24 μm long-term and short-term variable sources are shown in Appendices E and F, respectively.

$$Var = \frac{f_{\max} - f_{\min}}{\bar{f}} \times 100 \quad (2)$$

As can be seen from Table 3, the typical 24 μm *Var* values of the long-term and short-term variable sources are 37-43%, with typical errors of 12-13%. In Figure 8 we show *Var* against the mean 24 μm flux for each candidate (lower panel) with the typical errors (upper panel). The apparent lack of small values of *Var* at low 24 μm mean fluxes is because these sources have lower S/N detections and therefore higher errors in their photometry, and for the same variability they do not meet our χ^2 criterion. There is also a lack of large values of *Var* at high 24 μm mean fluxes. It is due to a statistical effect because the number of sources at high 24 μm mean fluxes is small, and the fraction of variable sources with low values of *Var* is higher than the fraction with large values of *Var*.

Finally, the reduced value of χ^2 , which is defined as χ^2/n with n being the number of epochs, has also been used as a measure of the 10 μm variability of local quasars by Neugebauer & Matthews (1999). For the long and short-term variable sources we find median χ^2/n values of 3.2 and 3.7, respectively. These are slightly higher than the values measured for local quasars at 10 μm . We note, however that our variability criterion in both cases is more restrictive than that used for the local quasars ($\chi^2/n > 1.5$).

It is not straightforward to compare our measures of the MIPS 24 μm variability in GOODS-South with studies done in the optical. The optical studies (e.g., Sarajedini et al. 2011; Villforth et al. 2010) used the variability significance and the variability strength as a measure of the variability. These parameters are defined in a different way than our *Var* and it is not appropriate to calculate them for our sources because they assume equal errors for all the sources, which is not the case for our epochs as shown in Section 2.

We can compare the MIPS 24 μm R_{\max} values with those measured in X-rays. Young et al. (2012) detected X-ray variable sources with maximum-to-minimum flux ratios $R_{\max} = 1.5 - 9.3$ with a median value of 4.1 over a period of 10.8 years. These values are noticeably higher than those measured at 24 μm both in short-term and long-term time scales. There are two explanations for this. First, as pointed out by Young et al. (2012), the limited photon statis-

tics of their X-ray observations means that sources must be strongly variable to be identified as such. The second reason is due to the reprocessed nature of the AGN mid-IR emission. Indeed, in the context of the AGN dusty torus, the IR variability of AGN is predicted to be only a fraction of the AGN intrinsic luminosity variation, to depend of the dust distribution, to be delayed with respect to optical variations, and to depend on the IR wavelength used (see Hönig & Kishimoto 2011 and references therein). This is because the dust is further away from the central engine than the accretion disk. This has been confirmed observationally for local quasars (Neugebauer & Matthews 1999) and Seyfert galaxies (Glass 2004).

5.3 IRAC colours

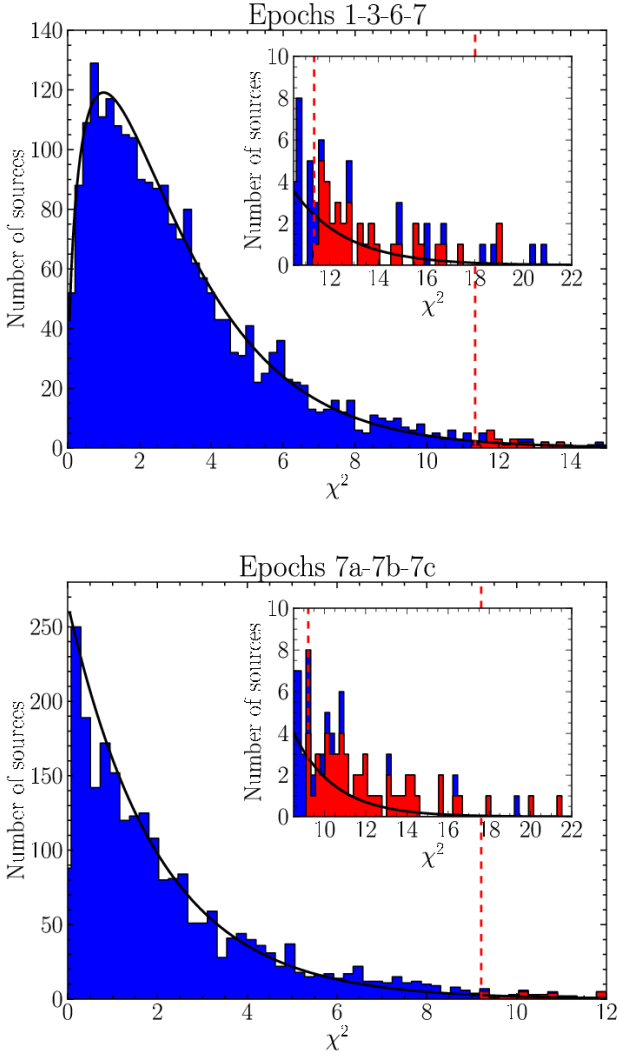
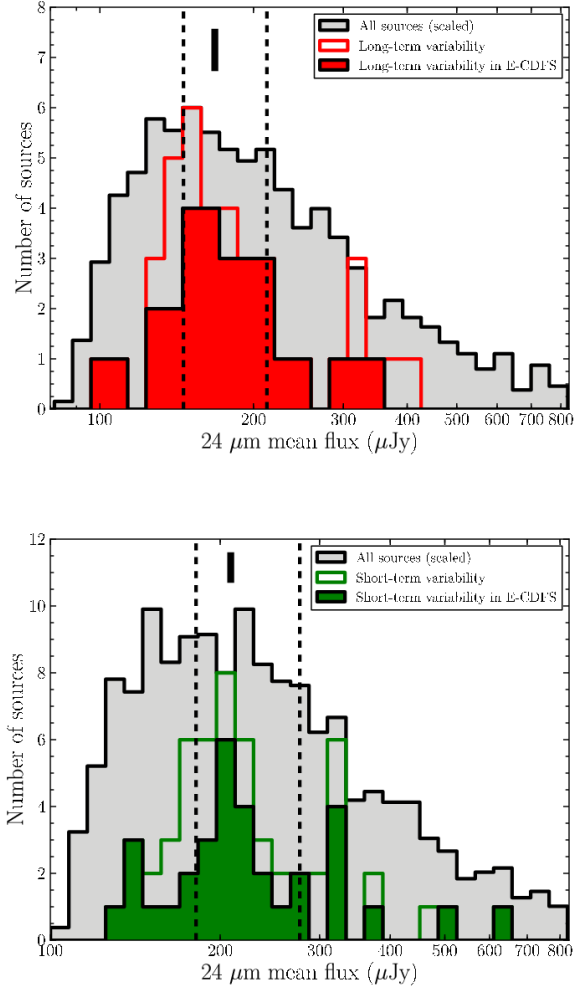
In this subsection we investigate the Spitzer-IRAC mid-IR (3.6, 4.5, 5.8, and 8.0 μm) properties of the MIPS 24 μm variable sources as the IRAC emission has also been used to select AGN candidates (e.g., Lacy et al. 2004; Stern et al. 2005; Alonso-Herrero et al. 2006; Donley et al. 2012; Lacy et al. 2013).

Lacy et al. (2004) defined a wedge in an IRAC colour-colour diagram to identify AGN via their IR emission, based on the locus of the diagram occupied by quasars. Donley et al. (2012) defined a more restrictive IRAC wedge based on the IR power-law criterion of Alonso-Herrero et al. (2006) and the typical errors of the IRAC photometry. This IR power-law wedge was specifically designed to avoid contamination from high-redshift star forming galaxies. To do so, Donley et al. applied a colour cut of $\log(S_{8.0}/S_{4.5}) > 0.15$ to avoid high-redshift ($z \geq 2$) star-forming galaxies. They also applied a vertical cut of $\log(S_{5.8}/S_{3.6}) > 0.08$ to prevent contamination due to low-redshift star-forming galaxies and required that the IRAC SED of the source rises monotonically. Donley et al. (2012) showed that this power-law wedge selects the majority of luminous X-ray identified AGN and therefore it is highly reliable at the expense of losing the least luminous AGN.

Finally, we note that recently Lacy et al. (2013) put forward a new expanded AGN selection criteria with a broader wedge when compared to that of Lacy et al. (2004) and im-

Table 3. Properties of the MIPS 24 μm variable sources.

Variability	f_{ν} 24 μm (μJy)		χ^2		Var (%)		R_{max}	
	Average	Median ¹	Average	Median ¹	Average	Median ¹	Average	Median ¹
Long-term	196	168 ¹⁴³ ₂₁₈	14.75	12.90 ^{11.94} _{15.46}	39.0	37.41 ^{28.3} _{43.7}	1.51	1.47 ^{1.33} _{1.57}
Short-term	239	209 ¹⁸¹ ₂₇₉	12.14	11.25 ^{10.23} _{13.67}	41.7	43.4 ^{29.5} _{49.2}	1.55	1.56 ^{1.36} _{1.66}

¹ Median and quartiles of the distribution.**Figure 3.** Observed χ^2 distributions (filled histograms) for all sources without neighbours within $10''$. The top panel is the distribution for the four epochs used for the long-term variability, whereas the bottom is for the three epochs used for the short-term variability. The black line is the theoretical χ^2 distribution for 3 degrees of freedom and 2 degrees of freedom, respectively. The dashed red line marks the 99th percentile for χ^2 due to random photometric errors alone. In the insets we zoom on the high χ^2 region. The red histograms show the χ^2 distribution for the final candidates after discarding problematic sources visually.**Figure 5.** Distribution of the 24 μm mean flux. The empty histograms are the distribution of the mean flux at 24 μm for long-term variable sources (top panel) and short-term variable sources (bottom panel) for the full sample, whereas the filled histogram are for sources in the E-CDFS (see Section 6). The black lines are the median and the dashed lines the first and third quartiles for the variable sources. The grey histograms shows the scaled distributions of all the sources detected in the four epochs (top) and three epochs (bottom) without neighbours within $10''$.

posed a 24 μm limit of $>600 \mu\text{Jy}$. We do not use this new wedge as only 1 short-term 24 μm variable source is above this limit (see Figure 5).

To obtain the IRAC data for our sources, we used the *Rainbow* Cosmological Surveys Database, which con-

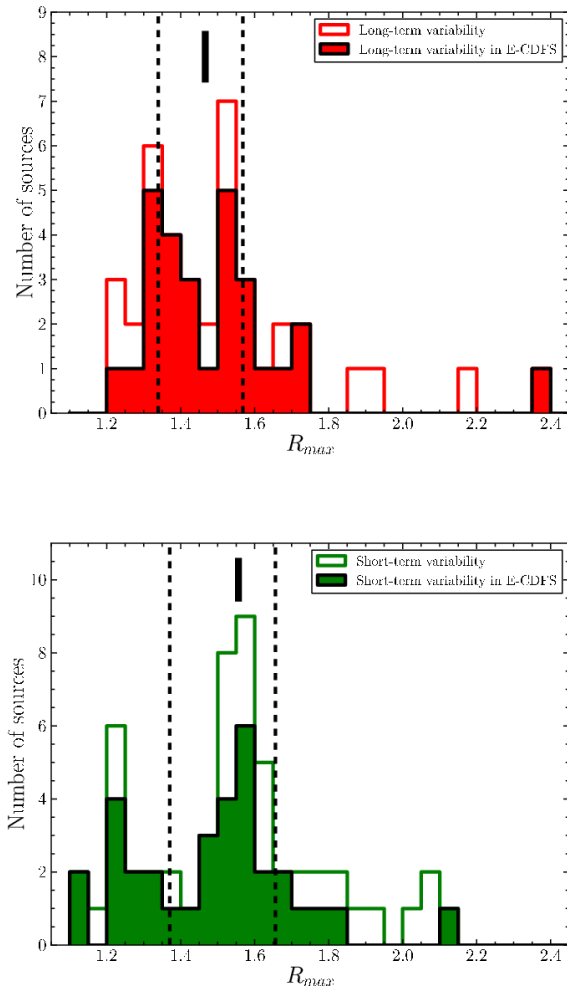


Figure 7. Distributions (open histograms) of the maximum to minimum flux ratio, R_{max} , for the MIPS 24 μm long-term variable sources (top panel) and short-term variable sources (bottom panel). The black lines correspond to the median and the dashed lines to the quartiles of the distributions. In both panels the filled histograms are the distributions for variable sources in the E-CDFS

tains multi-wavelength photometric data as well as spectroscopic information for sources in different cosmological fields, including GOODS-South (see Pérez-González et al. 2005, 2008). We cross-correlated the MIPS 24 μm catalogs with the *Rainbow* IRAC sources using a search radius of $2.5''$. Of the 39 long-term variable sources, 26 (67%) have a single counterpart and the remaining 13 (33%) have more than one counterpart within a radius of $2.5''$. Of the 55 short-term variable candidates, 44 (80%) have a single counterpart and the remaining 11 (20%) have more than one counterpart within a radius of $2.5''$. A visual inspection of the images at different wavelengths allowed us to identify the counterpart of the majority of the variable sources⁴. For the rest we used the data from the nearest source. All the long-term

⁴ In the majority of the sources, inspection of the IRAC images is enough to determine which source dominates in the IR.

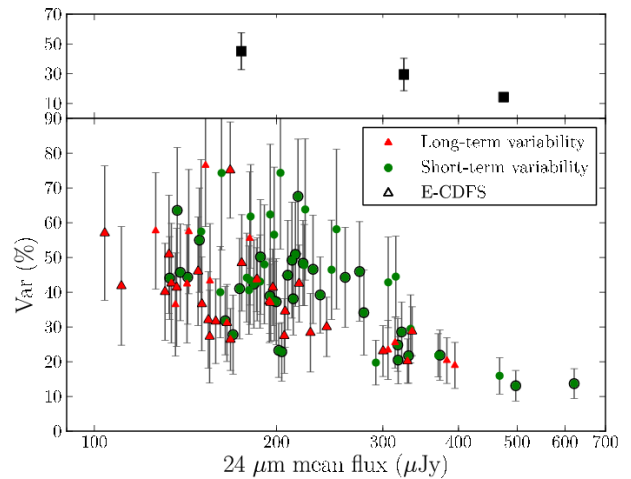


Figure 8. $Var = \frac{f_{max} - f_{min}}{f} \times 100$ as a function of the MIPS 24 μm mean flux for long-term variable sources (red filled triangles) and short-term variable sources (green filled circles). The black marked triangles/circles correspond to the variable sources in the E-CDFS. The top panel shows the average value of Var with its error for three flux intervals ($100 \mu\text{Jy} < F < 250 \mu\text{Jy}$, $250 \mu\text{Jy} < F < 400 \mu\text{Jy}$, $F > 400 \mu\text{Jy}$).

variable sources have fluxes in all four IRAC bands, whereas only 43 (78%) of 55 short-term variable candidates do. This is because the entire Epoch 7 region is not fully covered by the IRAC observations. The flux limits of the 24 μm variable sources are approximately $5 \mu\text{Jy}$ at $3.6 \mu\text{m}$, $4 \mu\text{Jy}$ at $4.5 \mu\text{m}$, $4 \mu\text{Jy}$ at $5.8 \mu\text{m}$, and $6 \mu\text{Jy}$ at $8 \mu\text{m}$.

Figure 9 shows the IRAC colour-colour plot for all the MIPS 24 μm variable sources detected in the four IRAC bands together with the Lacy et al. (2004) and Donley et al. (2012) AGN wedges. For comparison we also plot the IRAC colours of the full (non-variable) MIPS 24 μm sample in the common area of GOODS-South as grey dots. Of the 39 long-term variable sources, only 8% fall in the Donley et al. (2012) AGN region and 44% fall in the Lacy et al. (2004) AGN region. Of the 43 short-term variable sources with IRAC fluxes, 2% fall in the Donley et al. (2012) AGN region and 44% fall in the Lacy et al. (2004) AGN region. These fractions of mid-IR variable sources falling inside the Lacy et al. (2004) wedge are similar to those found for variable optical sources in GOODS-South (see Villforth, Sarajedini, & Koekemoer 2012). In an IRAC variability study Kozłowski et al. (2010) found a higher fraction (approximately 75%) of near-IR variable objects within an AGN wedge similar to that defined by Stern et al. (2005). This is most likely due to the relatively shallow IRAC observations of their study.

It is also worth noting that the fraction of objects in the parent MIPS 24 μm population in GOODS-South that are in the Lacy et al. (2004) wedge is 50%. However, the Lacy et al. (2004) AGN selection criteria was based on the IRAC colours of bright SDSS quasars with IRAC $8 \mu\text{m}$ fluxes greater than 1 mJy . In our general population, only about 1% of sources are above this limit. Alternatively, only 2% of the general sources in GOODS-South located inside the Lacy et al. (2004) wedge are found to be variable at 24 μm . Such a small fraction of mid-IR variable sources is expected,

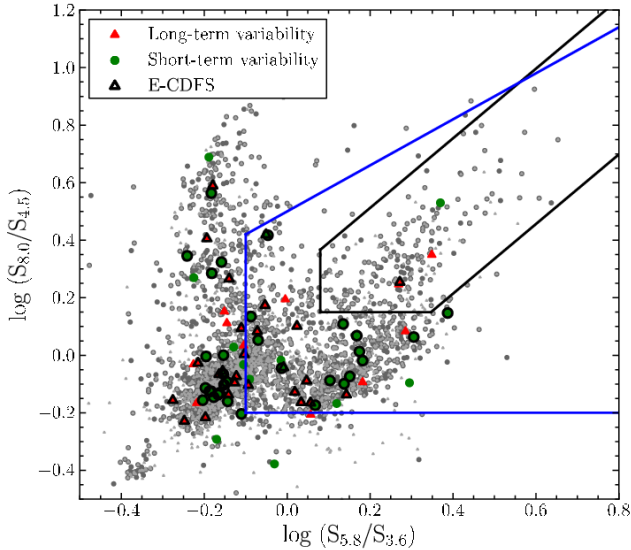


Figure 9. IRAC colour-colour plot of MIPS 24 μm sources in GOODS-South from the *Rainbow* database. The red filled triangles and green filled circles are the long-term and short-term MIPS 24 μm variable sources. The black marked triangles/circles mark the variable sources in the E-CDFS. The small grey dots are IRAC colours of the non-variable sources in the studied region. The different AGN wedges are shown as blue solid line for Lacy et al. (2004) and black solid line for Donley et al. (2012).

because the probability of detecting mid-IR variability of an AGN over the time scales probed and with three/four epochs is low. Additionally, it is likely that the AGN emission does not have a dominant contribution to the observed 24 μm emission.

6 CANDIDATES IN THE EXTENDED CHANDRA DEEP FIELD SOUTH

In this section we investigate the multi-wavelength properties of the MIPS 24 μm variable sources located in the Extended Chandra Deep Field South (E-CDFS), which is located in the central area covered by our study (see Figure 4). This field covers an area⁵ $\sim 1100 \text{ arcmin}^2$.

The E-CDFS was observed by COMBO-17 (Classifying Objects by Medium-Band Observations, a spectrophotometric 17-filter survey) survey (Wolf et al. 2004). The COMBO-17 object catalog contains, in addition to the 17 optical medium-band photometry, the broad-band $R_{\text{COMBO-17}}$ magnitude ($\lambda_c = 658 \text{ nm}$) and photometric redshifts for 63501 objects. We chose the E-CDFS because it has been observed with the deepest multi-wavelength data. We note that although the COMBO-17 catalog gives a photometric redshift, for the objects without spectroscopic redshift we use the photometric redshifts provided by the *Rainbow* database because they are calculated using both optical and

IR data (see Pérez-González et al. 2008). We only have spectroscopic redshifts for 8 long-term and 6 short-term variable objects.

For the cross-correlation we used again a search radius of 2.5". All the objects within this radius are possible counterparts. Since now we are looking at the same area we find relatively similar numbers of long (28) and short term (33) variable sources, although still the number of short term variable sources is higher due to the deepest central area of Epoch 7. Of the 39 long-term variable candidates, 28 are in the E-CDFS and 27 have a detection in the COMBO-17 catalog. Only 19 (70%) have a single counterpart, whereas the remaining 8 (30%) have more than one counterpart within a radius of 2.5". Of the 55 short-time variable candidates, 33 are in the E-CDFS and 28 are detected in the COMBO-17 catalog. Only 21 (75%) have a single counterpart and the other 7 (25%) have more than one counterpart in a radius of 2.5". In the following discussion in the case of multiple counterparts we associate the MIPS 24 μm source to the nearest object in the COMBO-17 catalog.

The COMBO-17 R -band magnitudes of the 24 μm variable sources are given in Tables C1 and D1 in the Appendices. The median values are $R\text{-band} = 22.6 \text{ mag}$ and $R\text{-band} = 22.3 \text{ mag}$ for the long and short-term variable sources, respectively (see Table 4). These values are similar to those of X-ray selected non-broad line AGN in deep cosmological fields whose optical luminosities are dominated by the host galaxy (Bauer et al. 2004). This is probably the case as well for the MIPS 24 μm variable sources as they are not dominated by the AGN (see next section).

We also searched for counterparts in the MUSYC (Multiwavelength Survey by Yale-Chile) catalog (Cardamone et al. 2010). See also Section 6.1. This catalog covers all the E-CDFS in the optical and near-IR. We used again a radius of 2.5" for the cross-correlation. We found 28 long-term variable sources detected in the MUSYC catalog, 23 (82%) of them with a single counterpart and 33 short-term variable sources, 31 (94%) with a single counterpart.

As a sanity check, we compared the variable MIPS 24 μm sources in the E-CDFS with the full variable catalog. We confirmed that their properties in terms of mean 24 μm fluxes (see Figure 5 and Tables 3 and 4) and the variability measures R_{max} and Var (see Figures 7 and 8) behave as the general 24 μm variable population. We therefore expect that the properties of the 24 μm variable sources in the E-CDFS might be extrapolated to the entire variable population.

6.1 Photometric redshifts and IRAC properties

In this section we study the distribution of the *Rainbow* redshifts for the MIPS 24 μm variable sources in the E-CDFS. For the long-term variable sources the redshifts are between 0.18 and 1.88 and for the short-term variable source between 0.12 and 1.94. This redshifts are in accordance with the redshifts of the MUSYC catalog. The average (median) redshifts are similar for the long-term $z = 0.94(0.90)$ and the short term $z = 0.96(1.00)$ variable sources. The average (median) redshifts for the sources in the MUSYC catalog are $z = 0.92(0.85)$ for the long-term and $z = 0.98(0.97)$ for the short-term variable candidates. We are therefore probing typically variable emission at 12 μm rest-frame. For comparison, the redshift distribution of the optical variable sources

⁵ The approximate location of this region compared to the region studied here can be seen from Figure 4 where we marked the MIPS 24 μm variable sources in the region of the E-CDFS

Table 4. Properties of MIPS 24 μm variable candidates in the E-CDFS.

Variability	No.	f_{ν} 24 μm (μJy)		χ^2		Var (%)		R_{max}		z		R_{mag}	
		Average	Median ¹	Average	Median ¹	Average	Median ¹	Average	Median ¹	Average	Median ¹	Average	Median ¹
Long-term	28	186	175 ¹⁵¹ ₂₀₇	14.98	12.90 ^{12.01} _{15.46}	38.1	37.4 ^{30.0} _{43.6}	1.49	1.46 ^{1.36} _{1.57}	0.94	0.90 ^{0.63} _{1.27}	22.66	22.63 ^{21.38} _{23.98}
Short-term	33	240	212 ¹⁸⁴ ₂₇₅	11.87	11.10 ^{10.23} _{12.52}	38.1	39.2 ^{27.8} _{45.9}	1.49	1.51 ^{1.33} _{1.60}	0.96	1.00 ^{0.53} _{1.28}	22.19	22.29 ^{21.01} _{23.49}

¹ Median and quartiles of the distribution.

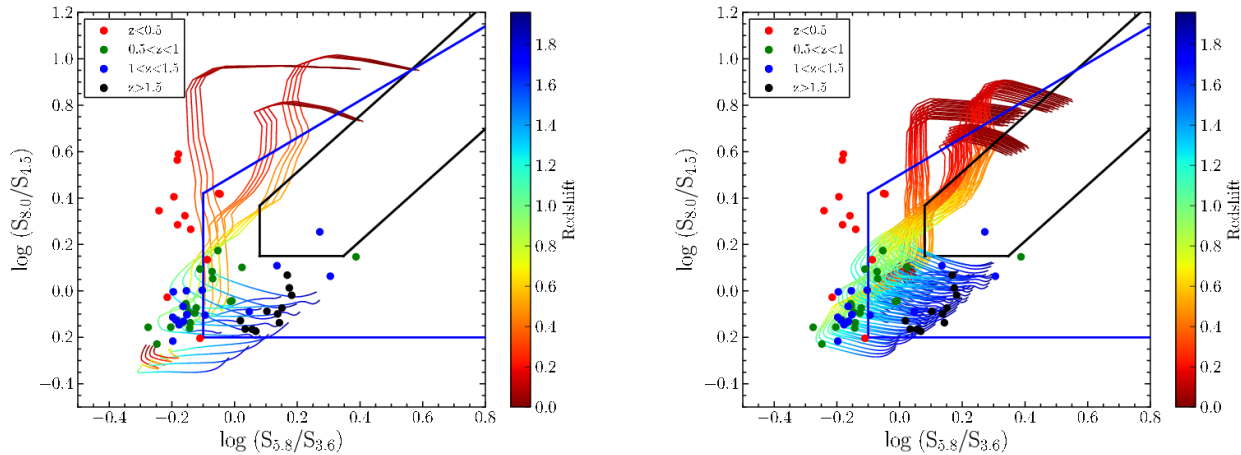


Figure 10. IRAC colour-colour plot of MIPS 24 μm variable sources in the E-CDFS, plotted according to their redshift. The multicoloured lines are the predicted IRAC colours of the star-forming templates from Donley et al. (2012) with a 20% AGN contribution (right panel) and no AGN contribution (left panel). The four sets of curves are for four different templates representing the galaxy contribution (see Donley et al. 2012 for more details). The redshift evolution from 0 (top of the curves) up to 2 (bottom of the curves) plotted (scale on the right hand side of the plots) is chosen to match the *Rainbow* z distribution of the MIPS 24 μm variable sources. The different AGN wedges are as in Figure 9.

in GOODS-South has a mean value 0.94 for i-band selected sources (Villforth et al. 2012) and 1.14 for v-band selected sources (Sarajedini et al. 2011). For the X-ray selected AGN in our parent 24 μm catalogs the average (median) redshift is $z = 1.08(0.78)$.

Figure 9 shows with black open symbols the IRAC colours of the MIPS 24 μm variable sources, both long and short term. As with the variability properties, the variable sources located in the E-CDFS behave as the general variable population, with approximately 50% being in the Lacy et al. (2004) wedge, and a small fraction in the Donley et al. (2012) wedge. As discussed above, the Donley et al. (2012) criteria are more restrictive to avoid contamination from star forming galaxies at different redshifts entering the AGN selection wedge but it misses a large fraction of low-luminosity AGN. In consequence, only one of the MIPS 24 μm variable sources in the E-CDFS would be classified as IR power-law galaxies according to Donley et al. (2012). Its ID is given in Table 5.

We can now use the redshift information in the IRAC colour-colour diagram to investigate whether variable sources in the Lacy et al. (2004) wedge can be classified as AGN, since the IRAC colours have a strong dependence with redshift. As shown in Figure 10, a large fraction of the MIPS 24 μm sources falling in the Lacy et al. (2004) wedge are at $z > 1$ (62% of the objects).

In Figure 10 we also plotted the tracks for an AGN/galaxy composite SED with a 20% AGN contribution (right panel) and no AGN contribution (left panel) with redshifts varying from 0 up to 2, and different degrees of extinction from Donley et al. (2012). As can be seen from these figures, the colours of approximately half of the MIPS 24 μm variable sources inside the Lacy et al. (2004) wedge agree with having a relatively small AGN fraction and are not compatible with a zero AGN fraction for their redshifts. This is similar to what is found for optical variable AGN in cosmological fields, where the AGN component is expected to be $\sim 10\%$ or less of the total galaxy flux in most cases (Sarajedini et al. 2011). Those outside this wedge might be compatible with just being normal galaxies (although see Section 6.2).

6.2 X-ray properties

One of the main goals of this work is to investigate whether variability at 24 μm is able to select AGN otherwise missed by deep X-ray exposures.

6.2.1 Fraction of 24 μm variable sources detected in X-rays

All the MIPS 24 μm variable sources, both long and short term, were matched against the deepest X-ray observations

in the CDFS, that is, the 4 Ms *Chandra* catalog presented in Xue et al. (2011), using again a search radius of $2.5''$. These deep observations cover only the central part of the E-CDFS. The rest of the area is covered by shallower X-ray observations that are part of the E-CDFS observations (see references listed in Table 5). We also cross-matched our variable sources with these shallower X-ray catalogs with a search radius of $2.5''$. We find 7 (25%) and 4 (12%) of the MIPS $24\mu\text{m}$ long-term and short-term variable sources respectively in the E-CDFS are detected in X-rays (see Table 5 for the ID of the sources). The lower fraction of X-ray detections among the short-term variable sources is because a large fraction of these are located outside the deepest 4 Ms X-ray region. These fractions of $24\mu\text{m}$ variable sources detected in X-rays are in general smaller than for AGN candidates selected by optical variability (30-50%) (Trevese et al. 2008; Sarajedini et al. 2011; Villforth et al. 2012).

In the central part of the E-CDFS (CDFS; $\sim 465\text{ arcmin}^2$), which is covered by the deepest X-ray data (Xue et al. 2011 catalog), 30% of the $24\mu\text{m}$ variable sources are detected in X-rays. Using the catalogs of Xue et al. (2011) and Lehmer et al. (2005, 2008), and the redshifts provided by the *Rainbow* Database, we find that the $24\mu\text{m}$ variable sources detected in X-rays have $0.5\text{--}8\text{ keV}$ luminosities ranging from $\sim 1 \times 10^{40}\text{ erg s}^{-1}$ to $\sim 1 \times 10^{44}\text{ erg s}^{-1}$ (See Table 5). Although some of our $24\mu\text{m}$ variable sources with an X-ray counterpart are low luminosity X-ray sources and would be below the limit X-ray luminosity for the AGN definition, this does not imply that these sources are not AGN. Young et al. (2012) studied sources classified as galaxies in X-rays and found the 22% of them presented variability in X-rays, confirming that variability selects AGN that might not be selected by other methods. There are also many optical variables that are not X-ray detected or that have low X-ray to optical flux ratios (see Fig 6 in Sarajedini et al. 2011).

6.2.2 Fraction of X-ray selected AGN found variable at $24\mu\text{m}$

As explained in the introduction, all AGN are expected to vary over a large range of timescales. However, the probability of detecting AGN variability in the mid-IR is always lower than the optical and near-IR because mid-IR variability is predicted to be only a fraction of the AGN intrinsic luminosity variation. This is because the dust responsible for the bulk of the mid-IR emission is further away from the central engine than the accretion disk, and the variability signal is expected to be smoothed for large dust distribution (see Neugebauer & Matthews 1999; Glass 2004; Hönig & Kishimoto 2011).

Before we compute the fraction of X-ray selected AGN found variable at $24\mu\text{m}$, we need to calculate the number of X-ray sources detected in $24\mu\text{m}$ satisfying our criteria in the parent catalogs as explained in Section 5.1. We found 211 X-ray sources in the central part of the E-CDFS (classified as AGN and galaxies in the Xue et al. (2011) catalog) satisfying the properties of our parent MIPS $24\mu\text{m}$ catalogs. Of these, only $\sim 4\%$ are found to be variable at $24\mu\text{m}$ on the timescales probed by our study. This fraction is smaller than the fraction found in the optical ($\sim 25\%$, see Klesman & Sarajedini 2007; Sarajedini et al. 2011). This is explained by model simulations, which predict a more smothered vari-

able signal and longer time scales in the mid-IR than in the optical (Hönig & Kishimoto 2011). In addition, for low luminosity AGN most of the mid-IR emission might come from the host galaxy, which would make it difficult to detect variability (see Section 6.1).

There are 149 sources classified as AGN in the Xue et al. (2011) catalog in our parent $24\mu\text{m}$ merged catalogs (see Section 5.1). If we assume that deep X-ray exposures provide the majority of the AGN in the field the total AGN population in this field would be 149 AGN. Assuming the $24\mu\text{m}$ variable sources in the region covered by the Xue et al. (2011) catalog not detected in X-ray are also AGN, they would only account for a small fraction ($\leq 13\%$) of the total AGN population in this field.

6.2.3 Candidates in the deepest X-ray region of the E-CDFS

As explained in Section 6.2.1, only the central area of the E-CDFS is covered by the deepest X-ray data (Xue et al. 2011). Since the effective exposure of the *Chandra* 4 Ms survey is not homogeneous (see Fig. 2 of Xue et al. 2011), we selected a central region of $\sim 115\text{ arcmin}^2$ with the deepest and most homogeneous X-ray coverage. In this region we can compare the sources in the parent catalog with the selected variable sources.

In this deepest X-ray region there are 189 sources in the parent $24\mu\text{m}$ long-term catalog and 181 in the parent $24\mu\text{m}$ short-term catalog. There are only 8 long-term variable sources and 5 short-term variable sources. Tables 6 and 7 summarize the results for the deepest X-ray region within the CDFS. As expected, the percentage of $24\mu\text{m}$ variable sources with an X-ray detection (63% for long-term and 60% for short-term variable sources) is higher than the percentage in our parent $24\mu\text{m}$ catalog sources detected in X-ray (48% for long-term and 55% for short-term variable sources). This is expected because the fraction of X-ray detection is higher in AGN than in not AGN. Since the number of variable sources in this region is small, the percentages given at Tables 6 and 7 suffer from small number statistics.

6.3 Monochromatic IR luminosities

From the *Rainbow* Database we obtained the rest-frame $24\mu\text{m}$ monochromatic luminosities for the MIPS $24\mu\text{m}$ variable sources. As the contribution of the AGN to the total luminosity in the $24\mu\text{m}$ variable sources is expected to be low (See Section 6.1), the luminosities were obtained by fitting the star forming galaxy templates from Chary & Elbaz (2001). Therefore, the fitted templates provide a reasonable approximation to the rest-frame $24\mu\text{m}$ luminosities of the sources, which arise from star formation in the host galaxy and the putative AGN. For each source we used all the available photometric mid-to-far IR data points to fit the SEDs. Apart from the MIPS $24\mu\text{m}$ flux, the *Rainbow* catalogs include photometry in the four IRAC bands, MIPS $70\mu\text{m}$ and *Herschel*/PACS 100 and $160\mu\text{m}$. For our sample of $24\mu\text{m}$ variable sources, 32% have $70\mu\text{m}$ photometry, 23% have $100\mu\text{m}$ photometry, and 18% have $160\mu\text{m}$ photometry.

Figure 11 shows these luminosities against the redshift for the long-term (red) and short-term (green) variable

Table 5. MIPS 24 μm variable sources identified with other AGN criteria.

ID	Catalogs	Ref	Lacy et al. (2004)	X-ray Luminosity (0.5-8 KeV) (erg s^{-1})
Long-term variable sources				
2552	X-ray, compilation AGN, optical-variable, IR power-law	(2), (3)*, (4), (5), (11), (13)	YES	1.20×10^{44}
13601	X-ray, Chandra 4 Ms, Radio excess	(2), (6), (9)*, (12)	NO	1.17×10^{42}
12099	X-ray	(3)*, (11)	NO	1.08×10^{43}
10015	relative IR SFR excess, X-ray	(7), (10)*	NO	8.88×10^{41}
2226	optical-variable, Chandra 4 Ms	(8), (9)*	NO	1.38×10^{40}
11976	Chandra 4 Ms	(9)*	YES	3.47×10^{42}
14779	Chandra 4 Ms	(9)*	NO	2.87×10^{40}
9796	Radio excess	(12)	YES	
9579	IR power-law	(13)	YES ¹	
4679	IR power-law	(13)	YES ¹	
Short-term variable sources				
8766	IR power-law, Chandra 4 Ms	(1), (9)*	YES	1.52×10^{41}
6827	X-ray, optical-variable, IR power-law	(2), (3)*, (5), (11), (13)	YES ¹	1.41×10^{42}
7761	X-ray, Chandra 4 Ms, Radio excess	(2), (6), (9)*, (12)	NO	1.17×10^{42}
7513	optical-variable	(8)	YES	
917	Chandra 4 Ms	(9)*	NO	2.36×10^{40}
2614	Chandra 4 Ms	(9)*	NO	3.66×10^{42}
540	Radio excess	(12)	YES ¹	

Notes.- References for the catalogs. (1) Alonso-Herrero et al. (2006); (2) Cardamone et al. (2008); (3) Lehmer et al. (2005) (4) Véron-Cetty & Véron (2010); (5) Trevese et al. (2008); (6) Tozzi et al. (2006); (7) Luo et al. (2011); (8) Villforth et al. (2010); (9) Xue et al. (2011); (10) Lehmer et al. (2008); (11) Silverman et al. (2010); (12) This work (radio excess); (13) This work (IR power-law according to Donley et al. (2012)).

* Reference for the X-ray luminosity.

¹ Not in the E-CDFS.

Table 6. Summary of fractions in the deepest X-ray region within the CDFS ($\sim 115 \text{ arcmin}^2$).

	No. sources parent 24 μm catalog	parent catalog with X-ray No. (%)	parent catalog with variability No. (%)	X-ray sources with variability No. (%)
Long-term	189	90 (48)	8 (4)	5 (6)
Short-term	181	99 (55)	5 (3)	3 (3)

candidates in the E-CDFS. The mean value of rest-frame $\log(\nu L_{24\mu\text{m}}/L_{\odot})$ is 10.5 for both, the long-term and the short-term variable sources. For those candidates satisfying the Lacy et al. (2004) AGN selection criteria the mean values are $\log(\nu L_{24\mu\text{m}}/L_{\odot}) = 10.7$ for both, the long-term and the short-term variable candidates. Conversely, the candidates not satisfying the Lacy et al. (2004) criteria have mean values of $\log(\nu L_{24\mu\text{m}}/L_{\odot}) = 10.3$ and 10.4 for the long-term and the short-term variable candidates, respectively. This is expected as galaxies in the Lacy et al. (2004) wedge tend to have a higher AGN fraction contributing to their IR emission than those outside (see previous section).

6.4 Radio properties

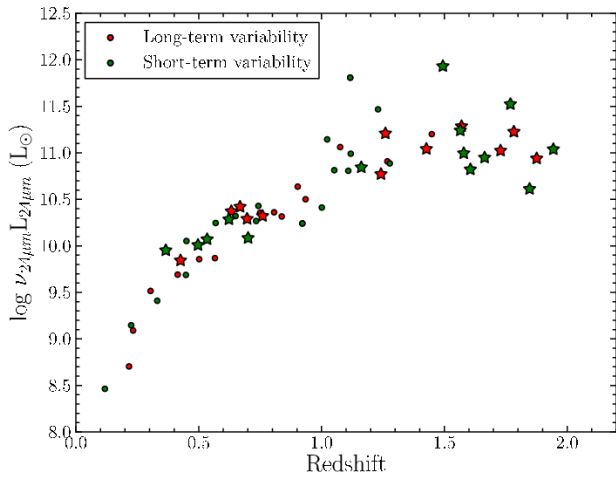
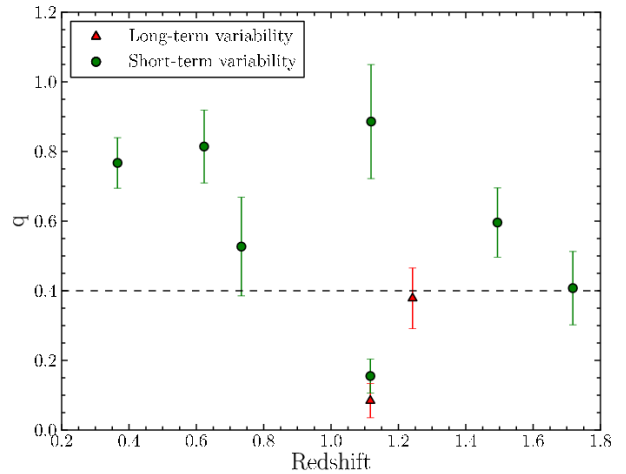
We investigate the radio properties of the MIPS 24 μm variable sources, since radio observations are in principle not biased against obscured AGN. Since star-forming galaxies

also emit at radio frequencies and show a tight correlation between the IR and the radio emission (e.g. Helou, Soifer & Rowan-Robinson 1985; Condon 1992; Ivison et al. 2010), it is also possible to select AGN in cosmological fields by looking for radio excess sources (see e.g. Donley et al. 2005; Del Moro et al. 2013). We cross-correlated our 24 μm variable sources with the Miller et al. (2013) radio 1.4 GHz source catalog and found that 2 long-term and 7 (one of which is outside the E-CDFS) short-term variable sources had a radio counterpart within a search radius of $2.5''$. That is, 7% and 18% of the MIPS 24 μm long and short term variable sources.

We calculated the q ratio defined as $q = \log(f_{24\mu\text{m}}/f_{1.4\text{GHz}})$ (see Appleton et al. 2004) to determine if any of these sources present a radio excess. Figure 12 shows q versus the redshift for the 14 MIPS 24 μm variable sources with radio detections at 1.4 GHz. Donley et al. (2005) considered radio excess sources those having $q < 0$ for non-K-corrected fluxes. On the other hand,

Table 7. Summary of fractions of MIPS 24 μm variable sources selected as AGN by other criteria.

	No. variable sources	X-ray ¹ No. (%)	radio ² excess No. (%)	other AGN ³ catalogs No. (%)	IR ⁴ power law No. (%)	Combined ⁵ No. (%)	Lacy et al. (2004) ⁶ criteria No. (%)	Combined ⁷ criteria No. (%)
Long-term variable sources								
Deepest X-ray region	8	5 (63)	1 (13)	3 (38)	0 (0)	5 (63)	3 (38)	7 (88)
In the E-CDFS	28	7 (25)	2 (7)	4 (14)	1 (4)	8 (29)	12 (43)	17 (61)
Outside the E-CDFS	11	0 (0)	0 (0)	0 (0)	2 (18)	2 (18)	5 (45)	5 (45)
In IRAC	39	7 (18)	2 (5)	4 (10)	3 (8)	10 (26)	17 (44)	22 (56)
All	39	7 (18)	2 (5)	4 (10)	3 (8)	10 (26)	17 (44)	22 (56)
Short-term variable sources								
Deepest X-ray region	5	3 (60)	1 (20)	2 (40)	0 (0)	3 (60)	2 (40)	4 (80)
In the E-CDFS	33	4 (12)	1 (3)	3 (9)	0 (0)	5 (15)	14 (42)	17 (52)
Outside the E-CDFS	22	1 (5)	1 (5)	1 (5)	1 (5)	2 (9)	5 (23)	5 (23)
In IRAC	43	5 (12)	2 (5)	4 (9)	1 (2)	7 (16)	19 (44)	22 (51)
All	55	5 (9)	2 (4)	4 (7)	1 (2)	7 (13)	19 (35)	22 (40)

¹ Variable MIPS 24 μm sources detected in X-rays.² Variable MIPS 24 μm sources with radio excess.³ Variable MIPS 24 μm sources in other AGN catalogs. (See notes in Table 5).⁴ Variable MIPS 24 μm sources detected as IR power-law AGN.⁵ Combined 1st, 2nd, 3rd, and 4th criteria.⁶ Variable MIPS 24 μm sources satisfying the Lacy et al. 2004 criteria.⁷ All the criteria combined.**Figure 11.** Rest-frame monochromatic 24 μm luminosity as a function of the redshift for the sources in the E-CDFS for long-term (red) and short-term (green) variable sources. The stars correspond to the variable sources satisfying the Lacy et al. (2004) AGN selection criteria**Figure 12.** The $q = \log(f_{24 \mu\text{m}}/f_{1.4 \text{ GHz}})$ ratio versus the redshift for long-term variable sources (red triangles) and short-term variable sources (green circles). Sources with $q < 0.4$ are considered to have a radio excess, as shown by Del Moro et al. (2013). Note we include a source out of the E-CDFS.

Del Moro et al. (2013) demonstrated that this limit misses a large fraction of sources with radio excesses based on the ratio between the far-IR luminosity and the radio emission. From Figure 5 of Del Moro et al. (2013), we can see that sources with $q < 0.4$ can be considered radio excess sources, and therefore AGN candidates. Among the MIPS 24 μm variable sources we find only 2 (7%) long-term and 2 (one of them out of the E-CDFS) (3%) short-term variable sources are radio excess sources, all of them at $z > 1.1$. Note that

we include the short-term source just above the line (see Figure 12). For reference, their IDs are given in Table 5. These small fractions of radio excess sources, if taken as AGN candidates among the MIPS 24 μm variable sources is generally consistent with the little overlap between radio selected AGN and AGN selected by their X-ray and/or IR emission in cosmological fields (Donley et al. 2005; Hickox et al. 2009; Villforth et al. 2012).

6.5 Comparison with other variability studies

Finally, we cross-correlated our 24 μm variable sources with sources found to be variable in other studies in the E-CDFS, using a search radius of $2.5''$. We found two long term and two short term variable sources at 24 μm in common with the optical variability studies of Trevese et al. (2008) and Villforth et al. (2010), and none with those of Cohen et al. (2006), Klesman & Sarajedini (2007), and Sarajedini et al. (2011). Three of these four sources are also detected in X-rays, as can be seen from Table 5. The low correspondence between optical and mid-IR variable sources is expected given the lags and lower variation of amplitude observed and predicted in the mid-IR for local AGN when compared with those observed in the optical (Neugebauer & Matthews 1999; Glass 2004; Hönig & Kishimoto 2011).

7 DISCUSSION AND SUMMARY

In this work we have used multi-epoch deep *Spitzer*/MIPS 24 μm observations in GOODS-South to look for mid-IR variable sources. The goal was to identify low luminosity and possibly obscured AGN candidates not identified by other methods. To select variable sources we used a χ^2 -statistics method to take into account the different photometric errors due to the different depths between epochs and varying depth within a given mosaic. By combining 24 μm data taken over three years and four epochs we studied long-term variability over time scales of months-years. Additionally we subdivided the longest duration epoch in three subepochs that allowed us to study the short-term variability in time scales of days over a period of seven days. In each epoch and subepoch, we restricted the analysis to sources above the 5σ detection limit and without neighbours at distances of less than $10''$ to minimize crowding effects in the photometry. We used a $2''$ cross-matching radius, imposing additionally that the $2''$ criterion was fulfilled in each pair of epochs.

After discarding problematic sources, our sample contains 39 long-term and 55 short-term mid-IR variability-selected AGN candidates over the GOODS-South areas of 1360 arcmin^2 and 1960 arcmin^2 , respectively, covered by the different epochs. The expected fraction of false positives in our sample of variable mid-IR sources is estimated to be about 40%. The mid-IR long and short-term variable sources comprise approximately 1.7% and 2.2% of the parent MIPS 24 μm samples, respectively. After removing the expected number of false positives the estimated percentages are 1.0% and 1.4%. These fractions of variable sources are typical of optical and near-IR variability studies in cosmological fields. The typical variability at 24 μm of the sources is 40%, both for the long and short-term variable sources.

In Section 6 we studied the properties of these variability selected AGN candidates restricting the region to the E-CDFS, as it contains the deepest and largest multi-wavelength coverage. We also made use of the *Rainbow* photometric redshifts that are calculated using optical and IR data for the objects without spectroscopic redshift. In the E-CDFS, we found 28 and 33 long and short term mid-IR variable sources, respectively, typically at $z = 1$ which implies our work is sensitive to variable emission at 12 μm rest-frame.

We cross-correlated our AGN candidates with other AGN catalogs including X-ray, radio, and variable catalogs in the E-CDFS. In the region with the best coverage by the deepest X-ray data, the *Chandra* 4 Ms catalog of Xue et al. (2011) (CDFS; $\sim 465 \text{ arcmin}^2$), 30% of the variable sources (both short and long term) are also detected in X-rays. However, their $0.5 - 8 \text{ keV}$ luminosities are typically $2 \times 10^{42} \text{ erg s}^{-1}$, with a few sources with X-ray luminosities of $\sim 10^{40} \text{ erg s}^{-1}$. In the *Chandra* 4 Ms catalog of Xue et al. (2011) there are 149 sources identified as AGN due to their X-ray luminosity in our parent MIPS 24 μm catalogs (i.e., after removing close neighbours and merging individual catalogs), see Section 5.1. If we assume that the 24 μm variable sources in the region covered by the Xue et al. (2011) catalog not detected in X-rays are AGN, they would only account for a small fraction ($\leq 13\%$) of the total AGN population in this field.

As expected, the fraction of 24 μm variable sources with a radio excess ($q = \log(f_{24 \mu\text{m}}/f_{1.4 \text{ GHz}}) < 0.4$) is small, as is the case with variable sources identified in other wavelengths. Table 7 summarizes the results.

We also investigated the IRAC properties of the 24 μm variable sources. The fraction of mid-IR variable selected AGN candidates meeting the Donley et al. (2012) IR power law criteria for AGN is small. This is not surprising, as this method has been proven to be a very reliable method to select luminous AGN, although it is highly incomplete for low luminosity X-ray selected AGN. Combining the AGN selected by the IR power law criteria with the above X-ray, radio, and variability criteria, we find that 29% and 15% of the long-term and short-term MIPS 24 μm variable sources would be also identified as AGN using other methods (see Table 7). The lower fraction for the short-term variable candidates is because a larger fraction of them lie in the area with the shallowest X-ray coverage (that is, the E-CDFS, see Section 6.2).

In Table 7 we also included the number of MIPS 24 μm variable sources that fall in the Lacy et al. (2004) IRAC colour-colour wedge. Approximately 44% of the 24 μm variable selected AGN candidates are located in this wedge. However, using their redshifts we concluded that of these only half of them would have colours compatible with a small ($\sim 20\%$) AGN contribution (see Section 6.1).

If we combined all these criteria together we would obtain an upper limit of $\sim 56\%$ to the fraction of MIPS 24 μm variable sources that would be identified as AGN by other methods. For reference in Table 7 we also listed these AGN fractions for sources outside the E-CDFS. However, as noted before the multi-wavelength coverage and depth of the observations outside this region are not as good, so these fractions should be taken as lower limits.

As explained in Section 6.2, only the central area of the E-CDFS is covered by the deepest X-ray data (Xue et al. 2011). We selected the region with the deepest and most homogeneous X-ray data ($\sim 115 \text{ arcmin}^2$), which is also covered by other AGN variability studies (Cohen et al. 2006; Klesman & Sarajedini 2007; Trevese et al. 2008; Villforth et al. 2010; Sarajedini et al. 2011). Combining all the criteria together, we obtained that $\sim 85\%$ of the 24 μm variable sources in this region would be identified as AGN by other methods (see Table 7). The percentage in this region is higher than when considering the entire E-CDFS due to

the deepest X-ray data and because other AGN catalogs do not cover all the E-CDFS. In this 115 arcmin² region we compared the parent catalog with the variable sources (see Table 6). As expected, in this region the fraction of 24 μ m variable sources with an X-ray detection is higher (63% for long-term and 60% for short-term variable sources) than that of sources in the parent 24 μ m catalog with X-ray detections (48% for long-term and 55% for short-term variable sources). Since the number of variable sources in this region is small, the percentages given at Tables 6 and 7 suffer from small number statistics.

In summary, we have shown that MIPS 24 μ m variability provides a new method to identify AGN in cosmological fields. We find, however, that the 24 μ m variable sources only account for a small fraction ($\leq 13\%$) of the general AGN population. This is expected because model simulations predict a more smothered variable signal and longer timescales in the mid-IR than in the optical (Hönig & Kishimoto 2011). Moreover, we found that the AGN contribution to the mid-IR emission of these 24 μ m variable sources is low (typically less than 20%). Since our method is only sensitive to high amplitude variability (see Section 4) then these 24 μ m variable sources are likely to host low-luminosity AGN where the variability is expected to be stronger (Trevese et al. 1994).

Acknowledgements

We thank the referee for valuable comments that helped improve the paper.

J.G.-G., A.A.-H., and A.H.-C. acknowledge support from the Augusto G. Linares research program of the Universidad de Cantabria and from the Spanish Plan Nacional through grant AYA2012-31447.

P.G.P.-G. acknowledges support from MINECO grant AYA2012-31277.

This work has made use of the Rainbow Cosmological Surveys Database, which is operated by the Universidad Complutense de Madrid (UCM), partnered with the University of California Observatories at Santa Cruz (UCO/Lick,UCSC). This research has made use of the NASA/IPAC Extragalactic Database (NED) which is operated by the Jet Propulsion Laboratory, California Institute of Technology, under contract with the National Aeronautics and Space Administration.

This work is based on observations made with the Spitzer Space Telescope, obtained from the NASA/ IPAC Infrared Science Archive, both of which are operated by the Jet Propulsion Laboratory, California Institute of Technology under a contract with the National Aeronautics and Space Administration.

REFERENCES

- Alexander D. M. et al., 2003, *AJ*, 126, 539
 Alexander D. M., & Hickox R. C., 2012, *NewAR*, 56, 93
 Alonso-Herrero A. et al., 2004, *ApJS*, 154, 155
 Alonso-Herrero A. et al., 2006, *ApJ*, 640, 167
 Antonucci R., 1993, *ARA&A*, 31, 473
 Appleton P. N. et al., 2004, *ApJS*, 157, 147
 Assef R. J. et al., 2013, *ApJ*, 772, 26
 Baldwin J. A., Phillips M. M., Terlevich R., 1981, *PASP*, 93, 5
 Balestra I. et al., 2010, *A&A*, 512, 12
 Bauer F. E., Alexander D. M., Brandt W. N., Schneider D. P., Treister E., Hornschemeier A. E., & Garmire G. P., 2004, *AJ*, 128, 2048
 Beckwith S. V. W. et al. 2006, *AJ*, 132, 1729
 Bertin E., Arnouts S., 1996, *A&AS*, 117, 393
 Brandt W. N., & Hasinger G., 2005, *ARA&A*, 43, 827
 Cardamone C. N. et al., 2008, *ApJ*, 680, 130
 Cardamone C. N. et al., 2010, *ApJS*, 189, 270
 Chary R., & Elbaz D., 2001, *ApJ*, 556, 562
 Cohen S. H. et al., 2006, *ApJ*, 639, 731
 Condon J. J., 1992, *ARA&A*, 30, 575
 Del Moro A., et al., 2013, *A&A*, 549, A59
 Donley J. L., Rieke G. H., Rigby J. R., Pérez-González P. G., 2005, *ApJ*, 634, 169
 Donley J. L. et al., 2012, *ApJ*, 748, 142
 Gandhi P., Horst H., Smette A., Hönig S., Comastri A., Gilli R., Vignali C., Duschl W., 2009, *A&A*, 502, 457
 Giacconi R. et al., 2001, *ApJ*, 551, 624,
 Giavalisco M. et al., 2004, *ApJ*, 600, L93
 Gilli R., Comastri A., & Hasinger G., 2007, *A&A*, 463, 79
 Glass I. S., 2004, *MNRAS*, 350, 1049
 Grazian A. et al., 2006, *A&A*, 449, 951
 Häring N., Rix H. W., 2004, *ApJ*, 604, L89
 Helou G., Soifer B. T., Rowan-Robinson M., 1985, *ApJ*, 298, 7
 Hickox R. C. et al., 2009, *ApJ*, 609, 891
 Hickox R. C., Mullaney J. R., Alexander D. M., Chen C. J., Civano F. M., Goulding A. D., Hainline K. N., 2014, *ApJ*, 782, 9
 Hönig S. F., Kishimoto M., 2011, *A&A*, 534, 121
 Hopkins A. M., Beacom J. F., 2006, *ApJ*, 651, 142
 Ivison R. J. et al., 2010, *A&A*, 518, 31
 Klesman A., Sarajedini V. L., 2007, *ApJ*, 665, 225
 Kormendy J., Richstone D., 1995, *ARA&A*, 33, 581
 Kozłowski S. et al., 2010, *ApJ*, 716, 530
 Lacy M. et al., 2004, *ApJS*, 154, L166
 Lacy M. et al., 2013, *ApJS*, 208, 24
 Le Fèvre O. et al., 2004, *A&A*, 428, 1043
 Lehmer B. D. et al., 2005, *ApJS*, 161, 21
 Lehmer B. D. et al., 2008, *ApJ*, 681, 1163
 Luo B. et al., 2011, *ApJ*, 740, 37
 Magorrian J. et al., 1998, *AJ*, 115, 2285
 Mainieri V. et al., 2008, *ApJS*, 179, 95
 Marconi A., Hunt L. K., 2003, *ApJ*, 589, L21
 Martínez-Sansigre A. et al., 2005, *Nature*, 436, 666
 Mateos S. et al., 2012, *MNRAS*, 426, 3271
 Mateos S., Alonso-Herrero A., Carrera F. J., Blain A., Severgnini P., Caccianiga A., Ruiz A., 2013, *MNRAS*, 434, 941
 Mignoli M. et al., 2005, *A&A*, 437, 883
 Mooley K. P., Frail D. A., Ofek E. O., Miller N. A., Kulkarni S. R., Horesh A., 2013, *ApJ*, 768, 165
 Miller N. A. et al., 2013, *ApJS*, 205, 13
 Moran E. C., Filippenko A. V., Chornock R., 2002, *ApJ*, 579, L71
 Neugebauer, G., & Matthews, K., 1999, *AJ*, 118, 35
 Paolillo M., Schreier E. J., Giacconi R., Koekemoer A. M., Grogin N. A., 2004, *ApJ*, 611, 93
 Pereyra N. A., Vanden Berk D. E., Turnshek D. A., Hillier

- D. J., Wilhite B. C., Kron R. G., Schneider D. P., Brinkmann J., 2006, ApJ, 642, 87
- Pérez-González P. G. et al., 2005, ApJ, 630, 82
- Pérez-González P. G. et al., 2008, ApJ, 675, 234
- Rieke G. H. et al., 2004, ApJS, 154, 25
- Sarajedini V. L., Gilliland R. L., Kasm C., 2003, ApJ, 599, 173
- Sarajedini V. L., Koo D. C., Klesman A. J., Laird E. S., Pérez-González P. G., Mozena M., 2011, ApJ, 731, 97
- Silverman J. D. et al., 2010, ApJS, 191, 124
- Smith M. G., Wright A. E., 1980, MNRAS, 191, 871
- Stern D. et al., 2005, ApJ, 631, 163
- Stern D. et al., 2012, ApJ, 753, 30
- Strolger L. G. et al., 2004, ApJ, 613, 200
- Tozzi P. et al., 2006, A&A, 451, 457
- Trevese D., Boutsia K., Vagnetti F., Cappellaro E., Puccetti S., 2008, A&A, 488, 73
- Trevese D., Kron R. G., Majewski S. R., Bershadsky M. A., Koo D. C., 1994, ApJ, 433, 494
- Ulrich M., Maraschi L., Urry C. M., 1997, ARA&A, 35, 445
- Veilleux S., Osterbrock D. E., 1987, ApJS, 63, 295
- Véron-Cetty M. P., Véron P., 2010, A&A, 518, 10
- Villforth C., Koekemoer A. M., Grogan N. A., 2010, ApJ, 723, 737
- Villforth C., Sarajedini, V., & Koekemoer A., 2012, MNRAS, 426, 360
- Werner M. W. et al., 2004, ApJS, 154, 1
- Williams R. E. et al., 1996, AJ, 551, 624
- Wolf C. et al., 2004, A&A, 421, 913
- Xue Y. Q. et al., 2011, ApJS, 195, 10
- Young M. et al., 2012, ApJ, 748, 124

APPENDIX A: PHOTOMETRIC ERRORS

As we explained in Section 4 errors are essential in the χ^2 method, and therefore we checked them in each epoch. For every source in each epoch, we calculated the ratio F_{epoch}/\bar{F} and $\Delta F_{epoch}/F_{epoch}$, where F_{epoch} is the flux in each epoch, \bar{F} is the mean flux for the source from measurements in all epochs, and ΔF_{epoch} is the error of the flux in each epoch. We separated the values in bins according to their mean flux value, so each bin contained 200 sources. For each bin we calculated the median of the F_i/\bar{F} values and $+1\sigma$ and -1σ (26th and 84th percentiles) so that between the median and $\sigma+$ there were the 34% of the data in the bin, and the same between the median and $\sigma-$. This is a measure of the scatter of the fluxes and should be consistent with the photometric errors. We also calculated the median of the $\Delta F_{epoch}/F_{epoch}$ for the sources of each bin.

Figure A1 plots the scatter in fluxes as a function of the 24 μm median flux for Epoch 1, as an example. As can be seen from the figure, the median of the errors (blue line) is consistent with the dispersion of the fluxes (red line). This confirms the validity of the estimated photometric errors used to calculate the χ^2 value. For all the epochs and sub-epochs these figures are similar and the photometric errors are consistent with the dispersion of the fluxes.

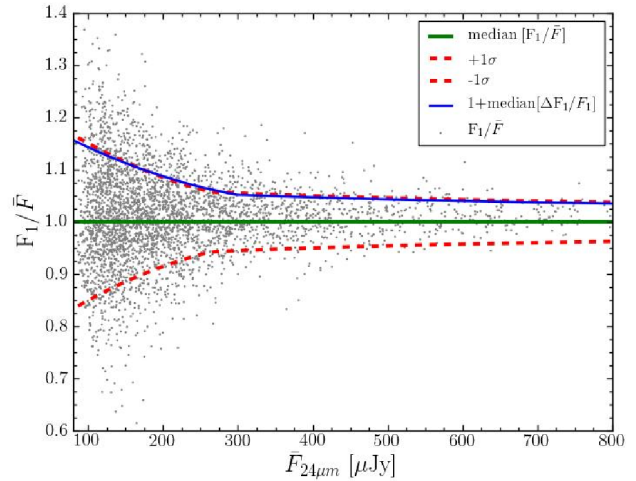


Figure A1. Scatter of the fluxes of the sources in epoch 1 (grey points). The black line represents the fit of the median in each bin and the red lines represent the fit of the $\pm 1\sigma$ (26th and 84th percentiles). The fit of the median of the photometric errors for each bin correspond to the blue line.

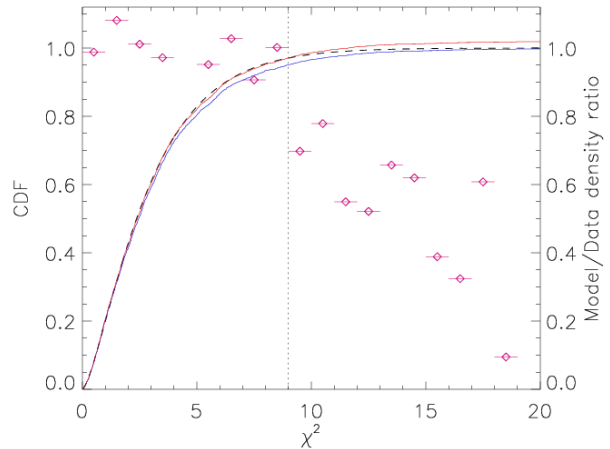


Figure B1. KS-test for the long-term data. The dashed line is the theoretical χ^2 distribution for 3 degrees of freedom corresponding to long-term variability. The blue line is the CDF of the data and the red line is the scaled and truncated CDF in $\chi^2=9$ (vertical dotted line). The magenta symbols (right axis) represent the ratio between the theoretical distribution of χ^2 and the number of sources in the sample, in intervals of $\Delta\chi^2=1$.

APPENDIX B: KOLMOGOROV-SMIRNOV TEST FOR χ^2 DISTRIBUTION

We performed a Kolmogorov-Smirnov test (hereafter KS-test) in order to determine whether our observed distributions of χ^2 values differ significantly from the theoretical distribution based on the assumption of gaussian photometric errors. We did the test for the data used to study both the long-term and short-term variability at 24 μm .

Figure B1 shows the cumulative distribution function, CDF, for the long-term data. As can be seen from the figure (and confirmed by a KS test), the theoretical χ^2 distribution for 3 degrees of freedom (dashed line) is incompatible with

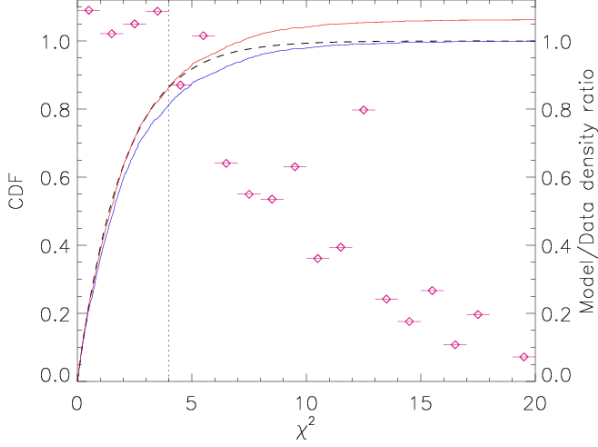


Figure B2. KS-test for the short-term data. The symbols are the same as Figure B1. In this case the dashed line corresponds to the theoretical χ^2 distribution for 2 degrees of freedom corresponding to short-term variability. The dotted line is the truncation of the CDF in $\chi^2=4$

the CDF of the data (blue line). This is because the tail of objects with high χ^2 is more populated than expected from the photometric errors alone. This is shown with the magenta symbols which are the ratio between the theoretical distribution of χ^2 and the number of sources in the sample, in intervals of $\Delta\chi^2=1$. This ratio presents a small deficit of sources in the range $\chi^2=1-2$ and an increasing excess at higher χ^2 values. We truncated and rescaled the CDF at $\chi^2=9$ (red line). The rescaled CDF follows well the theoretical distribution for $\chi^2 < 9$. There is a small depression around $\chi^2=5$, but it is not significant. The KS-test found no significant differences between the theoretical and the observed distributions below $\chi^2 < 9$. Cutting the CDF in $\chi^2=10$ the differences start to be significant. This indicates there is an excess of $\chi^2 > 9$ sources, which is evidence for variability.

Figure B2 shows the CDF for the short-term data. The theoretical distribution corresponds to a χ^2 distribution with 2 degrees of freedom. The rescaled CDF follows well the theoretical distribution for $\chi^2 < 4$. For higher values of χ^2 the difference between the theoretical and the observed distribution is significant, again indicating that our criterion is valid for selecting variable sources.

APPENDIX C: IMAGES OF THE VARIABLE CANDIDATES IN THE DIFFERENT EPOCHS

APPENDIX D: LONG-TERM VARIABLE CANDIDATES CATALOG

APPENDIX E: SHORT-TERM VARIABLE CANDIDATES CATALOG

APPENDIX F: LONG-TERM VARIABLE CANDIDATES LIGHT CURVES

APPENDIX G: SHORT-TERM VARIABLE CANDIDATES LIGHT CURVES

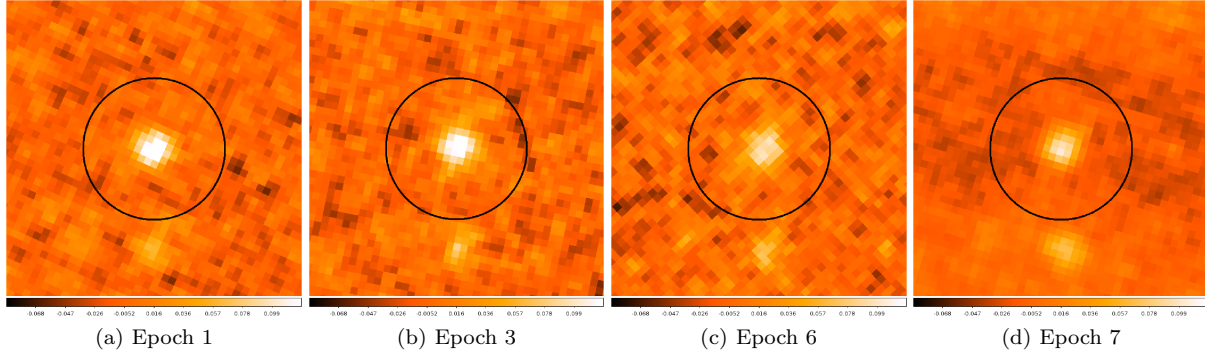


Figure C1. MIPS 24 μm images of the four epochs of the long-term variable candidate ID:5109. The FoV of the images is 50''x50''. The black circle represents the source and has a radius of 12''.

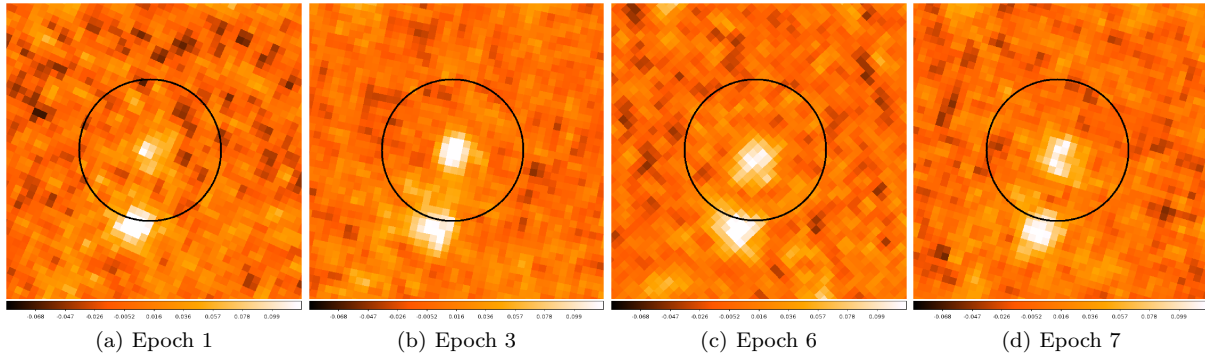


Figure C2. Same as Figure C1 for the long-term variable candidate ID:5086

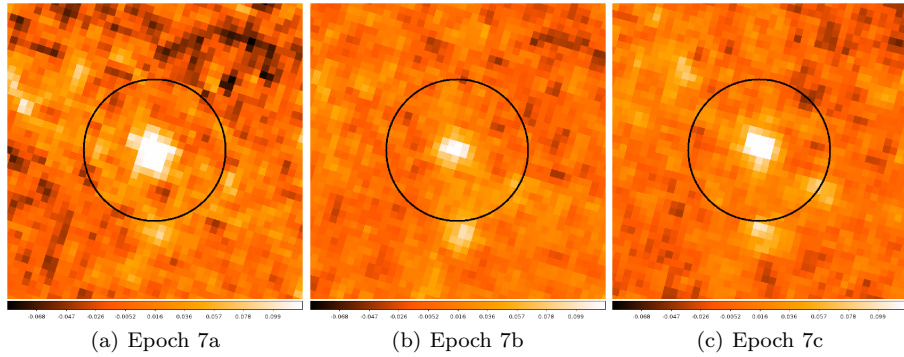


Figure C3. Same as Figure C1 for the short-term variable candidate ID:7513

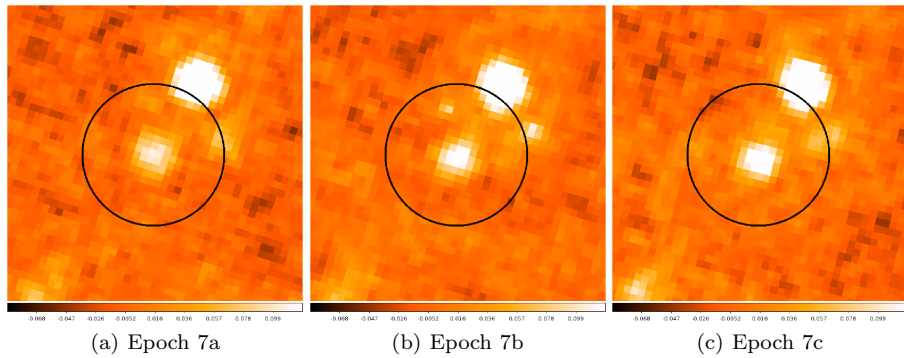


Figure C4. Same as Figure C1 for the short-term variable candidate ID:7921

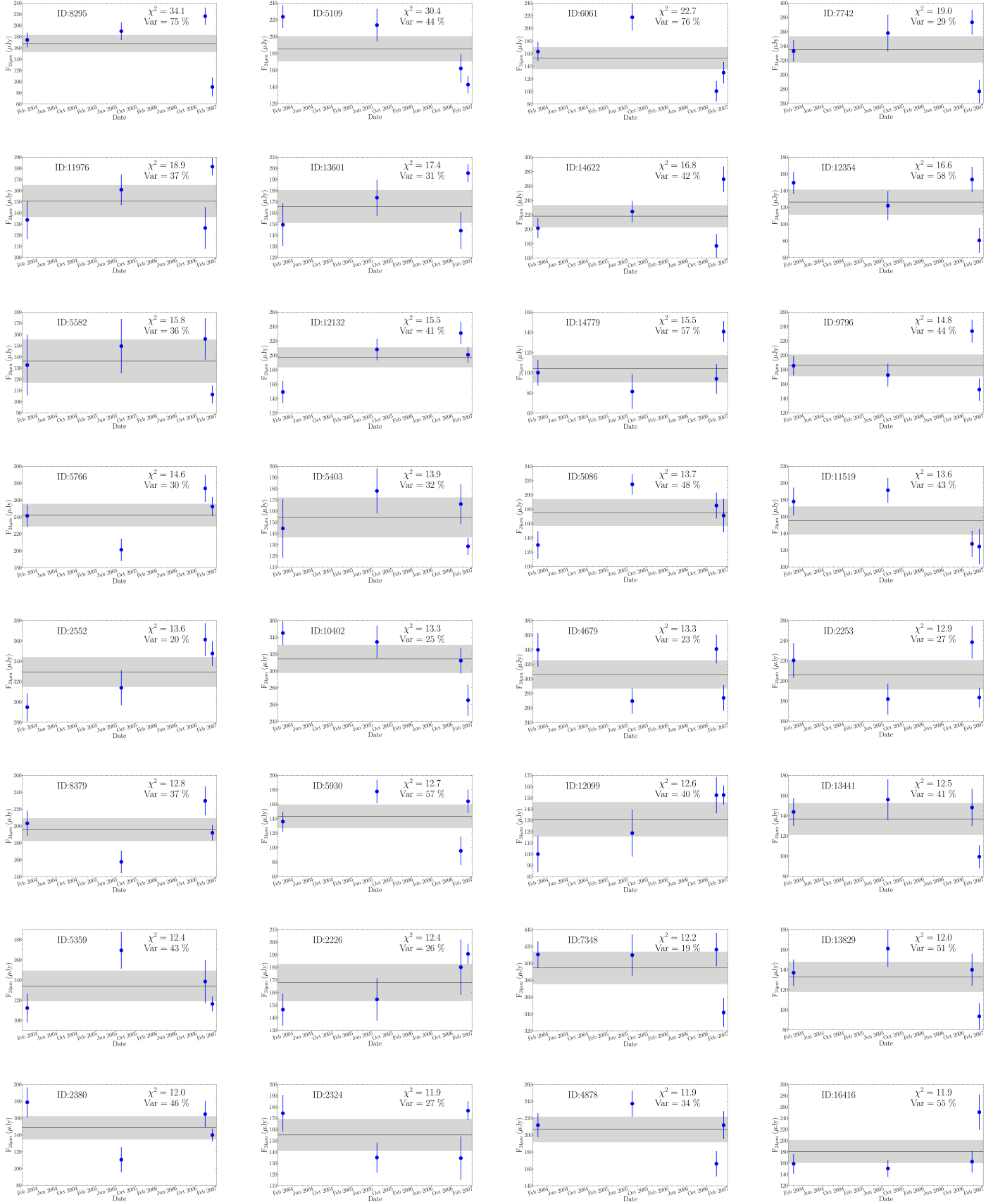
**Figure F1.** Light curves of MIPS 24 μm long-term variable candidates.

Table D1. Catalog of the long-term variable candidates.

ID	RA (J2000)	DEC (J2000)	Flux[epoch 1] (μ Jy)	Flux[epoch 3] (μ Jy)	Flux[epoch 6] (μ Jy)	Flux[epoch 7] (μ Jy)	\bar{F} (μ Jy)	χ^2	Var (%)	R_{max}	z^+	R	X-ray?	Radio?
7348	52.8655903	-27.5329591	410 \pm 16	410 \pm 24	416 \pm 20	342 \pm 17	395	12.23	18.9	1.22	0.71	-	NO	NO
13441* ^{1,2}	52.8882698	-27.7897526	144 \pm 14	156 \pm 20	148 \pm 18	99 \pm 11	137	12.48	41.4	1.57	0.57	20.98	NO	NO
5071*	52.9801950	-27.8067295	129 \pm 13	83 \pm 14	104 \pm 21	127 \pm 7	111	11.39	41.8	1.56	0.75	23.08	NO	NO
11519	53.0214235	-27.4722517	178 \pm 16	191 \pm 15	128 \pm 15	124 \pm 21	155	13.61	43.2	1.54	1.07	-	NO	NO
12269	53.0288333	-28.1259252	114 \pm 19	174 \pm 15	163 \pm 19	118 \pm 13	142	11.71	42.4	1.53	0.29	-	NO	NO
14622* ²	53.0467505	-27.5834456	201 \pm 14	225 \pm 14	177 \pm 16	269 \pm 18	218	16.75	42.5	1.52	1.43	25.22	NO	NO
9579	53.0534834	-27.4522969	403 \pm 17	418 \pm 17	341 \pm 19	369 \pm 21	383	11.63	20.3	1.23	0.19	-	NO	NO
16416	53.0543385	-27.3906117	159 \pm 17	151 \pm 15	163 \pm 19	251 \pm 31	180	11.87	55.5	1.67	0.57	-	NO	NO
5359*	53.0719302	-27.9225433	112 \pm 14	169 \pm 18	139 \pm 21	116 \pm 7	134	12.39	42.6	1.51	1.27	24.98	NO	NO
5080* ^{1,2}	53.0779999	-27.7740151	247 \pm 17	260 \pm 16	196 \pm 20	208 \pm 10	228	11.73	28.3	1.33	1.729	24.08	NO	NO
11976*	53.0885467	-27.8504550	134 \pm 17	161 \pm 14	126 \pm 19	182 \pm 8	151	18.92	36.6	1.44	1.78	23.28	YES	NO
9796* ^{1,2}	53.1110983	-27.6040756	185 \pm 13	172 \pm 16	234 \pm 16	152 \pm 15	186	14.77	43.7	1.53	1.24	24.79	NO	YES
5109* ²	53.1515045	-27.7620615	224 \pm 13	214 \pm 19	162 \pm 17	143 \pm 10	186	30.41	43.6	1.57	0.426	22.16	NO	NO
7742* ^{1,2}	53.1942822	-27.6723954	333 \pm 15	358 \pm 25	373 \pm 17	277 \pm 16	335	19.00	28.8	1.35	0.668	21.84	NO	NO
10015* ^{1,2}	53.1948840	-27.7538449	172 \pm 13	146 \pm 16	184 \pm 17	133 \pm 9	159	11.67	31.6	1.38	0.838	22.96	YES	NO
2226* ^{1,2}	53.2001248	-27.8155580	146 \pm 13	155 \pm 17	180 \pm 22	191 \pm 8	168	12.37	26.4	1.30	0.233	20.78	YES	NO
13601* ²	53.2022070	-27.8263358	149 \pm 19	174 \pm 16	144 \pm 16	196 \pm 8	166	17.41	31.1	1.36	1.117	25.08	YES	YES
14779* ^{1,2}	53.2047528	-27.7432269	100 \pm 13	81 \pm 17	94 \pm 15	141 \pm 10	104	15.46	57.0	1.73	0.216	19.75	YES	NO
2324* ²	53.2064728	-27.8675984	174 \pm 16	135 \pm 13	135 \pm 19	177 \pm 8	155	11.94	27.2	1.31	0.414	21.38	NO	NO
10402	53.2076102	-28.0760407	345 \pm 14	335 \pm 19	312 \pm 15	265 \pm 18	314	13.35	25.5	1.30	1.95	-	NO	NO
4679	53.2103280	-27.5243703	340 \pm 23	269 \pm 17	341 \pm 19	274 \pm 18	306	13.33	23.4	1.27	0.98	-	NO	NO
5930	53.2134267	-28.1566425	136 \pm 14	178 \pm 16	95 \pm 20	164 \pm 16	143	12.72	57.4	1.86	-	-	NO	NO
4878*	53.2139709	-27.6210732	212 \pm 14	273 \pm 15	166 \pm 15	212 \pm 16	207	11.88	34.5	1.43	1.88	-	NO	NO
10377* ¹	53.2681253	-28.0246684	198 \pm 19	169 \pm 16	171 \pm 25	241 \pm 17	195	11.58	37.4	1.43	0.92	22.83	NO	NO
2380* ^{1,2}	53.2730602	-27.8755176	179 \pm 18	111 \pm 15	165 \pm 15	140 \pm 8	149	12.01	46.0	1.62	0.50	20.99	NO	NO
12354	53.2756206	-28.0988060	149 \pm 13	122 \pm 17	153 \pm 15	81 \pm 15	126	16.58	57.6	1.90	1.86	-	NO	NO
8295*	53.2766409	-28.0183704	174 \pm 13	190 \pm 16	217 \pm 15	91 \pm 17	168	34.06	75.1	2.39	1.57	24.21	NO	NO
13829* ^{1,2}	53.2853000	-28.0627180	137 \pm 13	161 \pm 18	140 \pm 16	94 \pm 13	133	12.01	50.9	1.72	0.76	22.88	NO	NO
2552* ^{1,2}	53.2943522	-27.9635147	250 \pm 14	314 \pm 17	361 \pm 16	348 \pm 12	330	13.59	20.2	1.23	1.26	21.21	YES	NO
5086* ^{1,2}	53.2980525	-27.6902849	130 \pm 19	215 \pm 14	185 \pm 18	171 \pm 23	175	13.65	48.4	1.65	0.90	22.95	NO	NO
5451*	53.3000223	-27.8779051	283 \pm 18	345 \pm 16	275 \pm 15	298 \pm 10	300	11.82	23.1	1.25	0.81	22.52	NO	NO
2253* ^{1,2}	53.3011532	-27.7885025	220 \pm 17	182 \pm 15	239 \pm 16	184 \pm 10	206	12.90	27.4	1.31	1.45	23.98	NO	NO
12132* ¹	53.3266480	-27.8986874	149 \pm 15	208 \pm 15	231 \pm 15	201 \pm 10	197	15.46	41.4	1.55	0.63	21.31	NO	NO
5766* ²	53.3296181	-28.0256251	241 \pm 13	201 \pm 13	274 \pm 16	252 \pm 11	242	14.64	30.0	1.36	0.30	21.58	NO	NO
8379* ¹	53.3585985	-28.0450788	203 \pm 15	158 \pm 13	230 \pm 17	192 \pm 9	196	12.77	37.0	1.46	1.08	22.63	NO	NO
12099* ^{1,2}	53.3617713	-27.8518082	100 \pm 16	119 \pm 21	152 \pm 16	153 \pm 8	131	12.56	40.1	1.53	0.94	22.31	YES	NO
5403* ^{1,2}	53.3798560	-27.8245098	145 \pm 26	178 \pm 20	166 \pm 18	129 \pm 8	154	13.92	32.0	1.38	0.70	22.14	NO	NO
5582	53.4022377	-27.9101321	133 \pm 27	150 \pm 24	156 \pm 18	106 \pm 8	136	15.81	36.4	1.47	1.93	-	NO	NO
6061	53.4205850	-28.1435063	163 \pm 15	217 \pm 21	101 \pm 16	130 \pm 17	153	22.74	76.5	2.16	0.81	-	NO	NO

⁺ Redshifts with three decimal points are spectroscopic redshifts.

* In the E-CDFS.

¹ In COMBO-17 catalog and only one counterpart in 2.5'' in Rainbow catalog.

² Only one counterpart in 2.5'' in COMBO-17 catalog.

The references for the spectroscopic redshifts are: ID 5080: Grazian et al. (2006); ID 5109: Mignoli et al. (2005); ID 7742, 10015, 14779, 2324: Le Fèvre et al. (2004); ID 2226: Balestra et al. (2010); ID 13601: Mainieri et al. (2008).

Table E1. Catalog of the short-term variable candidates.

ID	RA (J2000)	DEC (J2000)	Flux [epoch7a] (μ Jy)	Flux [epoch7b] (μ Jy)	Flux7 [epoch7c] (μ Jy)	\bar{F} (μ Jy)	χ^2	Var (%)	R_{max}	z^+	R	X-ray?	Radio?
13	52.7297992	-27.5739281	298 \pm 30	216 \pm 33	156 \pm 33	223	10.80	63.8	1.92	-	-	NO	NO
2634* ^{1,2}	52.8866973	-27.8719379	211 \pm 15	229 \pm 15	155 \pm 17	198	11.81	37.5	1.48	0.65	20.30	NO	NO
6314* ^{1,2}	52.8931060	-27.8764410	200 \pm 14	194 \pm 15	128 \pm 21	174	10.12	41.0	1.56	0.74	21.20	NO	NO
937*	52.8942467	-27.8840075	326 \pm 14	281 \pm 14	346 \pm 16	318	10.15	20.5	1.23	1.16	-	NO	NO
2625* ²	52.8962139	-27.8649395	119 \pm 14	103 \pm 18	190 \pm 16	137	16.43	63.5	1.85	1.28	23.94	NO	NO
763*	52.9090009	-27.7866579	339 \pm 20	291 \pm 15	363 \pm 21	331	9.37	21.7	1.25	1.05	22.07	NO	NO
2356* ^{1,2}	52.9251368	-27.7383352	231 \pm 26	162 \pm 20	152 \pm 24	215	12.52	50.8	1.72	1.02	22.38	NO	NO
6827	52.9338732	-28.0834027	406 \pm 17	325 \pm 16	380 \pm 19	370	13.22	21.8	1.25	0.44	-	YES	NO
4648* ^{1,2}	52.9379937	-27.8746505	163 \pm 11	104 \pm 11	133 \pm 17	133	14.29	44.1	1.56	0.734	23.49	NO	YES
1947	52.9862313	-27.5157096	346 \pm 31	208 \pm 25	200 \pm 48	251	13.67	58.1	1.73	0.81	-	NO	NO
8181	52.9972222	-28.1038541	222 \pm 15	178 \pm 15	143 \pm 17	181	12.25	43.4	1.55	-	-	NO	NO
718* ^{1,2}	53.0047558	-27.7255025	243 \pm 26	149 \pm 20	235 \pm 31	209	11.87	44.9	1.63	1.001	22.29	NO	NO
7513* ^{1,2}	53.0134300	-27.7581000	272 \pm 19	165 \pm 18	227 \pm 18	221	16.47	48.3	1.65	0.534	21.01	NO	NO
917* ^{1,2}	53.0192273	-27.8352082	228 \pm 12	197 \pm 13	181 \pm 10	202	9.23	23.2	1.26	0.23	19.93	YES	NO
8613* ^{1,2}	53.0286682	-27.6356610	217 \pm 37	158 \pm 20	262 \pm 28	212	10.48	49.2	1.66	0.50	20.92	NO	NO
1943	53.0316927	-27.5017437	389 \pm 32	258 \pm 22	271 \pm 29	306	12.61	42.8	1.51	1.91	-	NO	NO
7921* ²	53.0476619	-27.9473127	173 \pm 15	212 \pm 12	254 \pm 16	213	13.81	38.1	1.47	1.11	22.21	NO	NO
2277*	53.0555289	-27.6597959	238 \pm 40	230 \pm 21	356 \pm 32	275	11.85	45.9	1.55	1.49	-	NO	YES
8766*	53.0819932	-27.7672103	369 \pm 17	321 \pm 18	277 \pm 22	322	11.94	28.5	1.33	0.62	-	YES	YES
517* ^{1,2}	53.0839618	-27.5734177	179 \pm 29	286 \pm 21	225 \pm 28	230	10.60	46.6	1.60	1.12	21.08	NO	YES
1503	53.0869545	-28.1404091	197 \pm 32	142 \pm 19	234 \pm 26	191	9.59	48.0	1.65	0.69	-	NO	NO
10885*	53.0925557	-27.9857229	360 \pm 18	311 \pm 15	282 \pm 16	318	11.10	24.8	1.28	0.57	-	NO	NO
6978	53.1064166	-28.1262429	389 \pm 24	307 \pm 19	249 \pm 27	315	15.63	44.5	1.56	1.03	-	NO	NO
185* ^{1,2}	53.1121892	-28.0514201	341 \pm 18	354 \pm 22	423 \pm 20	373	10.06	21.9	1.24	1.57	24.00	NO	NO
3265*	53.1250338	-28.0383985	234 \pm 25	191 \pm 16	140 \pm 18	188	10.79	50.2	1.68	1.85	23.61	NO	NO
4501* ^{1,2}	53.1367677	-27.7688610	610 \pm 20	669 \pm 19	584 \pm 18	621	10.60	13.7	1.15	0.366	20.36	NO	YES
2091	53.1518662	-27.5393472	257 \pm 31	145 \pm 21	194 \pm 30	198	9.93	56.5	1.78	0.28	-	NO	NO
2847* ^{1,2}	53.1549571	-27.8767845	234 \pm 11	192 \pm 11	187 \pm 13	204	10.23	22.8	1.25	0.331	20.49	NO	NO
1925	53.1620312	-27.4562601	222 \pm 28	243 \pm 25	121 \pm 29	195	11.14	62.4	2.01	1.00	-	NO	NO
3702	53.1828042	-28.2246423	293 \pm 38	142 \pm 20	175 \pm 29	203	15.70	74.3	2.07	-	-	NO	NO
7761* ^{1,2}	53.2024886	-27.8262335	227 \pm 14	208 \pm 14	151 \pm 16	195	14.12	38.9	1.50	1.117	25.08	YES	YES
4477* ¹	53.2235604	-27.7345674	253 \pm 18	274 \pm 17	182 \pm 19	236	14.08	39.2	1.51	1.58	23.97	NO	NO
540	53.2480035	-27.5404651	139 \pm 27	114 \pm 20	235 \pm 28	162	13.26	74.3	2.06	1.72	-	NO	YES
2614* ^{1,2}	53.2610999	-27.7598248	106 \pm 13	141 \pm 17	169 \pm 13	139	11.25	45.7	1.60	1.23	23.34	YES	NO
6876*	53.2681484	-28.0248935	129 \pm 23	246 \pm 20	276 \pm 26	217	21.45	67.6	2.13	0.92	22.83	NO	NO
6017*	53.2758295	-27.6029799	206 \pm 28	321 \pm 24	253 \pm 30	260	10.25	44.3	1.56	1.77	23.94	NO	NO
2409* ^{1,2}	53.2795549	-27.6633534	322 \pm 27	227 \pm 20	288 \pm 32	279	9.23	34.1	1.42	0.45	21.35	NO	NO
10903*	53.2826321	-27.9443909	200 \pm 16	237 \pm 17	163 \pm 18	200	9.24	37.2	1.46	0.12	20.91	NO	NO
1209* ^{1,2}	53.2846948	-27.9283298	176 \pm 13	139 \pm 15	113 \pm 14	143	11.46	44.3	1.56	0.70	21.66	NO	NO
7869* ^{1,2}	53.3057210	-27.8438699	185 \pm 10	186 \pm 15	138 \pm 13	170	9.86	27.8	1.34	0.32	19.51	NO	NO
8106*	53.3173805	-27.9729970	178 \pm 13	225 \pm 17	148 \pm 16	184	11.56	42.3	1.53	0.45	22.63	NO	NO
6918* ^{1,2}	53.3352837	-28.0254291	108 \pm 17	150 \pm 13	190 \pm 14	149	14.42	55.0	1.76	1.61	23.41	NO	NO
8050* ²	53.3430057	-27.9321166	480 \pm 19	539 \pm 16	474 \pm 15	498	10.33	13.1	1.14	1.66	23.43	NO	NO
123*	53.3747793	-27.8008735	164 \pm 10	139 \pm 12	191 \pm 11	165	10.80	31.8	1.38	1.94	-	NO	NO
3632	53.3868526	-28.1329288	303 \pm 28	189 \pm 21	249 \pm 26	247	11.93	46.5	1.61	0.62	-	NO	NO
10053	53.4529616	-27.8423718	322 \pm 13	265 \pm 14	290 \pm 12	292	9.62	19.7	1.22	-	-	NO	NO
2734	53.4539570	-27.7478151	162 \pm 16	187 \pm 24	101 \pm 19	150	9.70	57.4	1.85	0.48	-	NO	NO
1032	53.4584105	-27.7783558	168 \pm 17	191 \pm 16	126 \pm 14	162	10.35	40.0	1.51	1.05	-	NO	NO
6622	53.4639456	-27.8334061	507 \pm 18	464 \pm 21	432 \pm 17	468	9.30	15.9	1.17	-	-	NO	NO
4767	53.4656628	-27.7659261	134 \pm 14	212 \pm 17	190 \pm 16	179	14.28	44.1	1.59	0.11	-	NO	NO
1039	53.4768023	-27.7778086	168 \pm 19	244 \pm 17	132 \pm 20	181	20.08	61.8	1.85	-	-	NO	NO
6814	53.4846854	-27.9221903	180 \pm 18	144 \pm 14	217 \pm 18	180	10.95	40.6	1.51	-	-	NO	NO
5284	53.4862820	-27.9564971	225 \pm 20	144 \pm 14	195 \pm 15	188	13.10	43.0	1.56	-	-	NO	NO
7936	53.4911453	-27.8278011	363 \pm 23	269 \pm 26	368 \pm 19	333	10.89	29.5	1.37	-	-	NO	NO
12955	53.4921523	-27.8248350	212 \pm 14	175 \pm 16	281 \pm 20	222	17.93	47.8	1.61	-	-	NO	NO

⁺ Redshifts with three decimal points are spectroscopic redshifts.

* In the E-CDFS.

¹ In COMBO-17 catalog and only one counterpart in 2.5'' in Rainbow catalog.² Only one counterpart in 2.5'' in COMBO-17 catalog.

The references for the spectroscopic redshifts are: ID 4648, 2847: Le Fèvre et al. (2004); ID 718, 7513: Balestra et al. (2010); ID 4501: Mignoli et al. (2005); ID 7761: Mainieri et al. (2008).

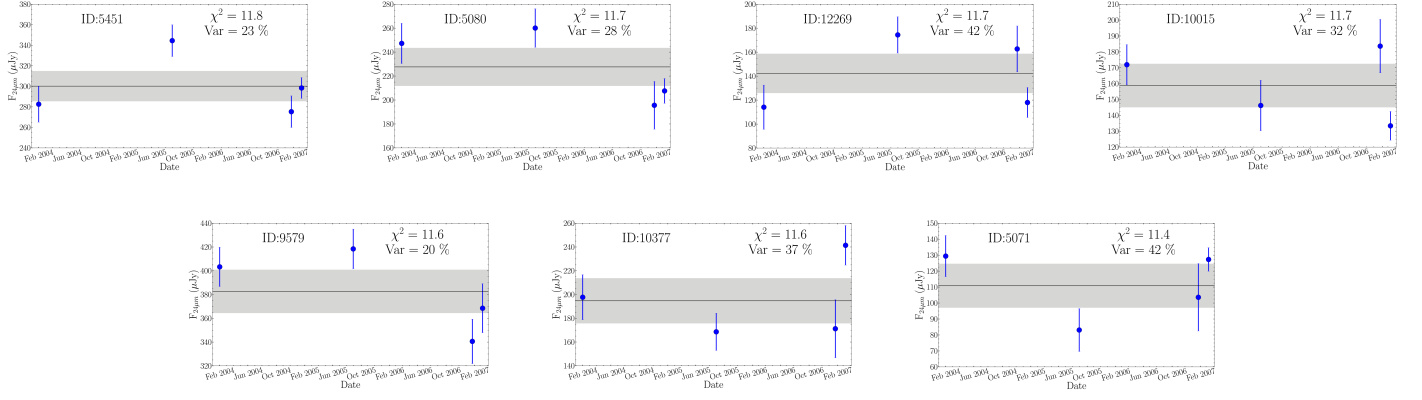
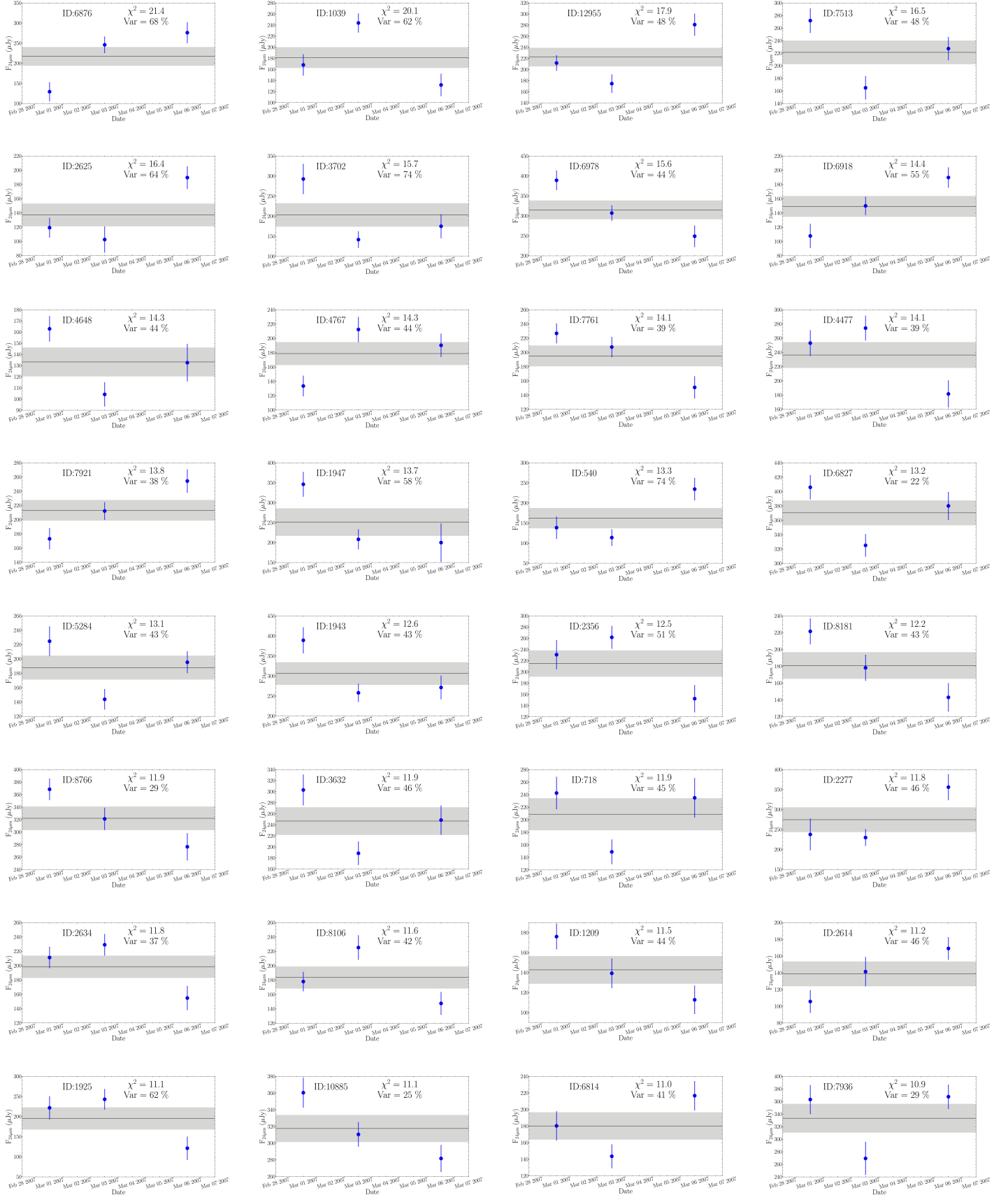


Figure F1 – continued

**Figure G1.** Light curves of MIPS 24 μm short-term variable candidates.

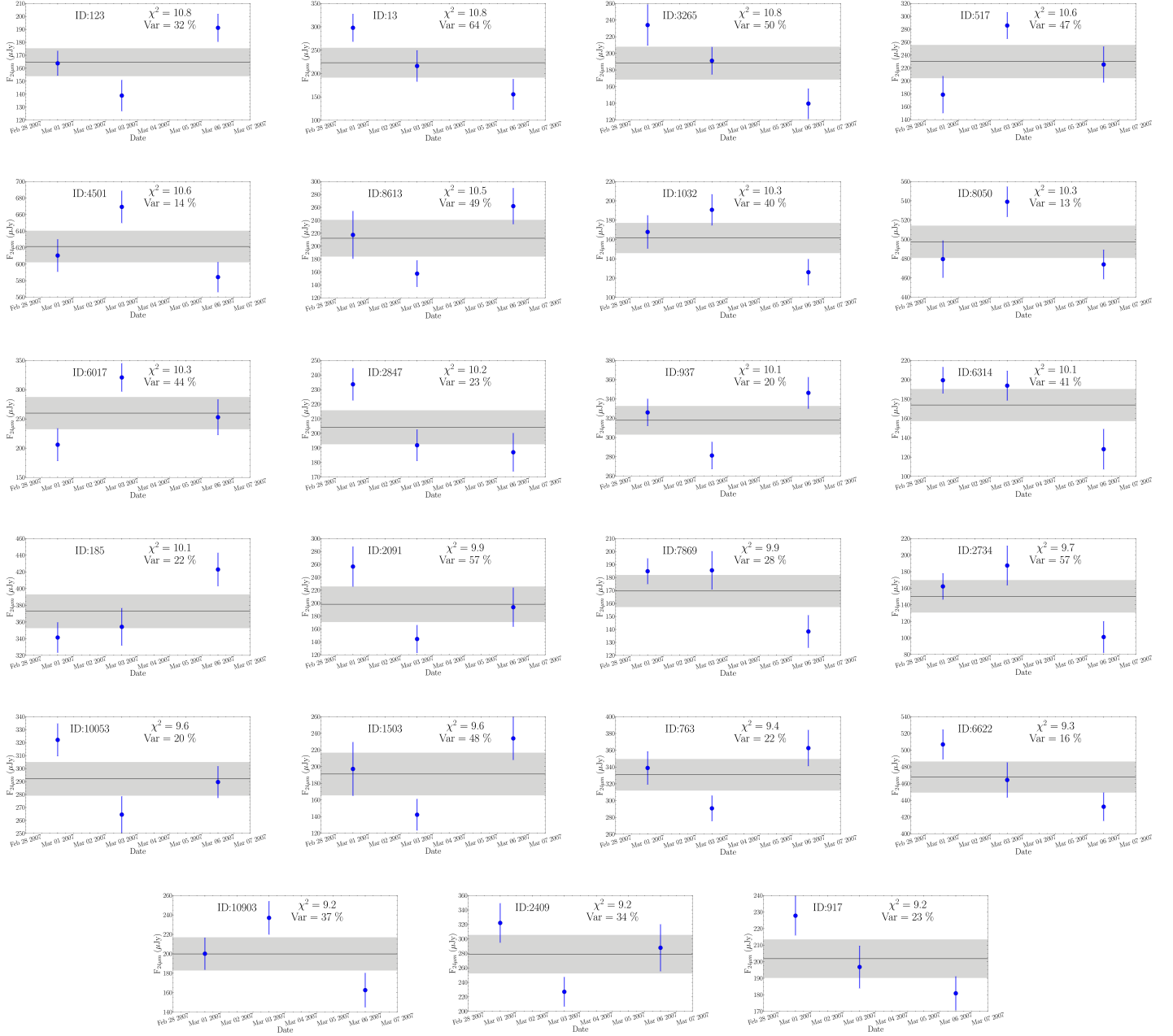


Figure G1 – continued